Phosphoproteome Analysis Identifies a Synaptotagmin-1-Associated Complex Involved in Ischemic Neuron Injury

Authors

Wei Jiang, Pei Zhang, Peng Yang, Na Kang, Junqiang Liu, Yilixiati Aihemaiti, and Haijun Tu

Correspondence

haijuntu@hnu.edu.cn

In Brief

To investigate the role of protein modification in the hippocampus after cerebral ischemia onset, we used a quantitative proteomics approach to study proteome and phosphoproteome profiles of the acute cerebral ischemic hippocampus in middle cerebral artery occlusion mouse model. Bioinformatic analysis revealed that phosphoproteins fall into a variety of biological processes of synaptic components and neurotransmission. Moreover, functional analysis identifies a synaptotagmin-1-associated complex in mediating ischemic neuron injury.

Graphical Abstract

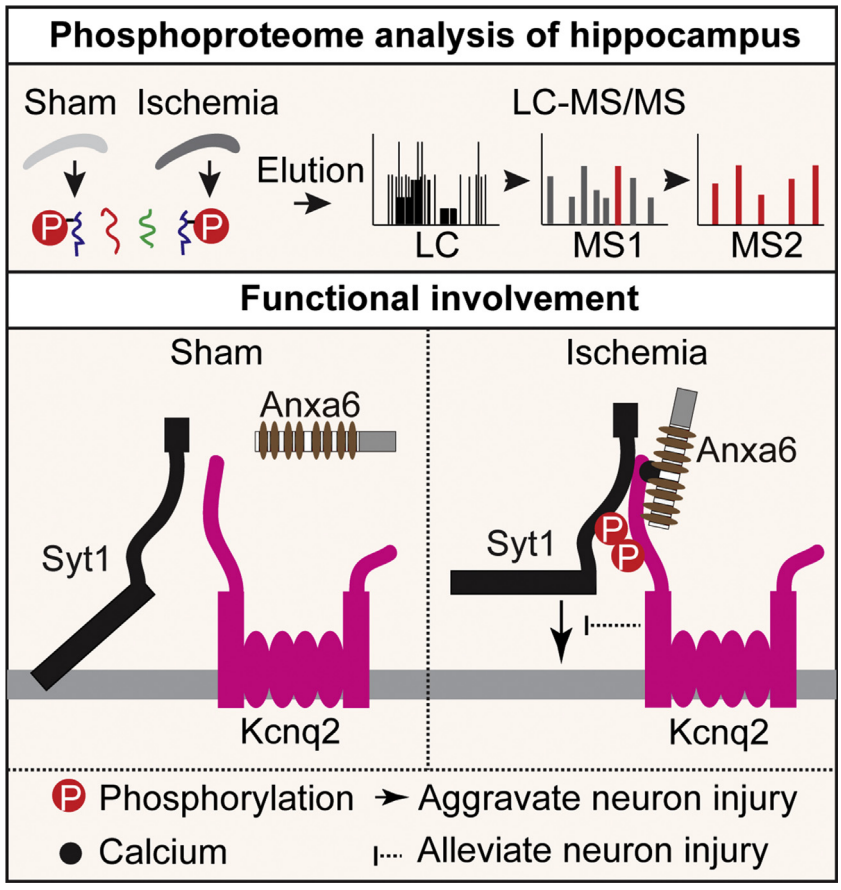

Highlights

- Established the phosphoproteome profiles of acute cerebral ischemic hippocampus.
- Phosphoproteomic profile reveals phosphorylation of Syt1 and Kcnq2, which are upregulated.
- Phosphorylation of Syt1 aggravates neuron injury, which is relieved by Tat-Syt1^{T112A}.
- Kcnq2 interacts with Syt1 and Anxa6 and alleviates Syt1-mediated neuronal injury.

2022, Mol Cell Proteomics *21*(*5*), 100222

https://doi.org/10.1016/j.mcpro.2022.100222

Phosphoproteome Analysis Identifies a Synaptotagmin-1-Associated Complex Involved in Ischemic Neuron Injury

Wei Jiang[1,2], Pei Zhang[1,2], Peng Yang[1,2], Na Kang[1,2], Junqiang Liu[1,2], Yilixiati Aihemaiti[1,2], and Haijun Tu[1,2,*]

Cerebral stroke is one of the leading causes of death in adults worldwide. However, the molecular mechanisms of stroke-induced neuron injury are not fully understood. Here, we obtained phosphoproteomic and proteomic profiles of the acute ischemic hippocampus by LC–MS/MS analysis. Quantitative phosphoproteomic analyses revealed that the dysregulated phosphoproteins were involved in synaptic components and neurotransmission. We further demonstrated that phosphorylation of Synaptotagmin-1 (Syt1) at the Thr112 site in cultured hippocampal neurons aggravated oxygen-glucose deprivation–induced neuronal injury. Immature neurons with low expression of Syt1 exhibit slight neuronal injury in a cerebral ischemia model. Administration of the Tat-Syt1^{T112A} peptide protects neurons against cerebral ischemia-induced injury *in vitro* and *in vivo*. Surprisingly, potassium voltage-gated channel subfamily KQT member 2 (Kcnq2) interacted with Syt1 and Annexin A6 (Anxa6) and alleviated Syt1-mediated neuronal injury upon oxygen-glucose deprivation treatment. These results reveal a mechanism underlying neuronal injury and may provide new targets for neuroprotection after acute cerebral ischemia onset.

Cerebral stroke is a serious cerebrovascular event that is a major cause of adult disability and mortality worldwide. Approximately, 80% of strokes are due to cerebral ischemia, which occurs when an embolus or thrombus blocks the major cerebral artery, resulting in cell death (1). Currently, treatments against cerebral stroke are mainly preventive due to the lack of effective therapeutic methods. Although recombinant tissue plasminogen activator is an important medicine to treat cerebral ischemia by dissolving the obstructive clot to restore blood flow within 4.5 h after the onset of stroke symptoms, cerebral ischemia-induced neuronal injury or death is the major cause of cerebral infarction, leading to an irreversible neurological deficit after cerebral stroke (1).

Although a series of complex biochemical incidents, including excitotoxicity, ionic imbalance, oxidative stress, apoptosis, and inflammation following cerebral ischemia, lead to neural injury, irreversible damage, and even neural death (2), the biological events that may be potential targets for neuroprotection of cerebral ischemia in acute phases are not fully understood. Recent advances in phosphoproteomic and proteomic technologies offer opportunities to study the global phosphorylated protein and protein landscape of various samples in a single experiment (3–6). Neurons in the cortex, striatum, and hippocampal region are highly vulnerable to cerebral ischemia, and the proteome of the cortex and striatum after cerebral ischemia has been established (7–12). To further uncover the biological events in the hippocampus involved in cerebral ischemia-induced neuronal injury, we used the mouse hippocampus of a focal cerebral ischemia model and monitored changes in phosphorylated protein abundance using a combination of stable isotope labeling and high-resolution LC–MS/MS to systematically profile the phosphoproteome and proteome after acute cerebral ischemia onset. Quantitative phosphoproteomic analyses revealed dysregulated phosphoproteins associated with synaptic component and neurotransmission. We further demonstrated that phosphorylation of the synaptic protein synaptotagmin 1 (Syt1) at the Thr112 site in cultured hippocampal neurons aggravated oxygen-glucose deprivation (OGD)-induced neuronal injury. Administration of the Tat-Syt1^{T112A} peptide protects neurons against cerebral ischemia-induced injury *in vitro* and *in vivo*. Interestingly, the potassium voltage-gated channel subfamily KQT member 2 (Kcnq2) interacted with Syt1 and Annexin A6 (Anxa6) and alleviated Syt1-mediated neuronal injury upon OGD treatment. Our data serve as a broad resource for probing the acute ischemia neuron phosphoproteome, reveal a molecular mechanism underlying neuron injury in cerebral ischemia, and may also provide new targets for neuroprotection upon acute cerebral ischemia onset.

From the [1]State Key Laboratory of Chemo/Biosensing and Chemometrics, College of Biology, and [2]Shenzhen Research Institute, Hunan University, Shenzhen, Guangdong, China

*For correspondence: Haijun Tu, haijuntu@hnu.edu.cn.

https://doi.org/10.1016/j.mcpro.2022.100222

EXPERIMENTAL PROCEDURES

Experimental Design and Statistical Rationale

For proteomic analysis, focal cerebral ischemia for 2 h was induced by intraluminal middle cerebral artery occlusion (MCAO). Ten hippocampus each after sham or acute MCAO ischemia for 2 h were analyzed by three biological replicate MS runs (3–4 hippocampus each after sham or acute MCAO ischemia were pooled as a technical replicate in individual biological replicate). Five percent (40 μg) of the pool was used for whole proteome analysis, and the remaining 95% (760 μg) was subjected to phosphoproteome profiling. Kyoto Encyclopedia of Genes and Genomes (KEGG) pathway analysis of upregulated based on fold changes in phosphorylation of >1.2, *t* test, *p* value <0.05, KEGG pathway analysis of downregulated based on fold changes in phosphorylation of <1/1.2, *t* test, *p* value <0.05.

Animal

C57BL/6J male mice on postnatal day 56 ± 3 days old (P56) were used and housed individually under standard conditions of temperature and humidity and a 12 h light/dark cycle with free access to food and water. C57BL/6J male mice on postnatal day 14 ± 2 days old (P14) were used as immature mice. All animal experiments were conducted in strict accordance with the Guide for the Care and Use of Laboratory Animals (Eighth Edition). All experimental protocols were reviewed and approved by the Institutional Animal Care and Use Committee of Hunan University.

Focal Cerebral Ischemia Model

Focal cerebral ischemia was induced by intraluminal MCAO (13). Briefly, mice were anesthetized with 5% isoflurane and maintained with 1% isoflurane (R511-22, RWD Life Science) in an oxygen/air mixture by using a gas anesthesia mask (R580S, RWD Life Science). The left common carotid artery and the external carotid artery (ECA) were exposed by a ventral midline neck incision and clipped. The ECA was ligated with a 5-0 silk suture, and a 2-cm long silicon-rubber-coated monofilament (MSMC24B104PK50, RWD Life Science) was advanced from the ECA through the internal carotid artery up to the level of the anterior cerebral artery (both P14 and P56 mice). The suture was inserted 9 mm from the bifurcation of the common carotid artery to occlude the middle cerebral artery (MCA) to induce permanent cerebral ischemia. The sham-operated animals were treated identically, except that the middle cerebral artery was not occluded after the neck incision.

Protein Extraction

The sample was ground in liquid nitrogen into cell powder and then transferred to a 5-ml centrifuge tube. After that, four volumes of lysis buffer (8 M urea, 1% Protease Inhibitor Cocktail) were added to the cell powder, followed by sonication three times on ice using a high-intensity ultrasonic processor. The remaining debris was removed by centrifugation at 12,000*g* at 4 °C for 10 min. Finally, the supernatant was collected, and the protein concentration was determined with a bicinchoninic acid assay kit according to the manufacturer's instructions.

Trypsin Digestion

For digestion, the protein solution was reduced with 5 mM DTT for 30 min at 56 °C and alkylated with 11 mM iodoacetamide for 15 min at room temperature in darkness. The protein sample was then diluted by adding 100 mM triethylamine bicarbonate to urea concentrations less than 2 M. Finally, trypsin was added at a 1:50 trypsin-to-protein mass ratio for the first digestion overnight and a 1:100 trypsin-to-protein mass ratio for a second 4 h digestion.

TMT Labeling

After trypsin digestion, the peptide was desalted by a Strata X C18 SPE column (Phenomenex) and vacuum-dried. Peptide was reconstituted in 0.5 M triethylamine bicarbonate and processed according to the manufacturer's protocol for the tandem mass tag (TMT) kit. Briefly, one unit of TMT reagent was thawed and reconstituted in acetonitrile. The peptide mixtures were then incubated for 2 h at room temperature and pooled, desalted, and dried by vacuum centrifugation.

Affinity Enrichment

To enrich phosphorylation-modified peptides, peptide mixtures were first incubated with immobilized metal-ion affinity chromatography (IMAC) microsphere suspensions with vibration in loading buffer (50% acetonitrile/6% TFA). The IMAC microspheres with enriched phosphopeptides were collected by centrifugation, and the supernatant was removed. The IMAC microspheres were washed with 50% acetonitrile/6% TFA and 30% acetonitrile/0.1% TFA to remove nonspecifically adsorbed peptides. Then, the elution buffer containing 10% NH4OH was used to elute the enriched phosphopeptides from the IMAC microspheres, and the enriched phosphopeptides were eluted with vibration. The supernatant containing phosphopeptides was collected and lyophilized for LC–MS/MS analysis.

Liquid Chromatography-Tandem Mass Spectrometry

The tryptic peptides were dissolved in 0.1% formic acid (solvent A) and followed by loaded onto a homemade reversed-phase analytical column (15-cm length, 75 μm i.d.). The gradient was comprised of an increase from 6% to 23% solvent B (0.1% formic acid in 98% acetonitrile) over 26 min, 23% to 35% in 8 min and climbing to 80% in 3 min, then holding at 80% for the last 3 min, all at a constant flow rate of 400 nl/min on an EASY-nLC 1000 UPLC system. The peptides were subjected to an NSI source followed by tandem mass spectrometry (MS/MS) in a Q ExactiveTM Plus (Thermo) coupled online to UPLC. The electrospray voltage of 2.0 kV was applied, and the m/z scan range from 350 to 1800 was used for full scan, and intact peptides were detected in the Orbitrap at a resolution of 70,000. Peptides were then selected for MS/MS using the NCE setting of 28, and the fragments were detected in the Orbitrap at a resolution of 17,500. A data-dependent procedure was alternated with one MS scan followed by 20 MS/MS scans with 15.0 s dynamic exclusion. Automatic gain control was set at 5E4, and fixed first mass was set as 100 m/z. Carbamidomethyl on cysteines was specified as fixed modification. Acetylation on protein N-terminal and oxidation on methionine were specified as variable modifications for proteome. Acetylation on protein N-terminal, oxidation on methionine, and phosphorylation on serine, threonine, and tyrosine were specified as variable modifications for phosphoproteome. Three biological replicates of sham and cerebral ischemia showed that the median value of RSD <0.05, which was calculated by three experiments SDs demonstrated the reliability of quantification measurement between biological replicates were good.

Database Search

The resulting MS/MS data were processed using the MaxQuant search engine (v.1.5.2.8). Tandem mass spectra were searched against the SwissProt Mouse database (released February 2018;16,964 sequences) concatenated with the reverse decoy database. Trypsin/P was specified as a cleavage enzyme allowing up to four missing cleavages. The mass tolerance for precursor ions was set as 20 ppm in the first search and 5 ppm in the main search, and the mass tolerance for fragment ions was set as 0.02 Da. False discovery rate was adjusted to <1%, and the minimum score for modified peptides was set >40.

Quantitative Analysis of Proteome and Phosphoproteome

The raw LC-MS datasets were first searched against database and converted into matrices containing reporter intensity of peptides across samples. For proteome quantitative analysis, the relative quantitative value of each protein was calculated based on these intensity values, and the intensities of peptide (I) across all samples were centralized and transformed into their values of relative quantification (U) in each sample and was calculated by the formula, where i denotes the sample and j denotes the peptide. $U_{ij} = I_{ij}/Mean(I_j)$. The relative quantitative value of peptide be corrected by median value as follows: $NR_{ij} = U_{ij}/Median(U_j)$ to adjust the systematic bias of the identified peptide amount among different samples in the process of mass spectrometry detection. The relative quantitative value of a protein (R) is calculated by the intensity median of its corresponding unique peptides. The formula is listed as follow where k denotes the protein and j denotes the unique peptides belonging to the protein: $R_{ik} = Median(NR_{ij}, j \in k)$.

For phosphoproteome quantitative analysis, the relative quantitative value of each modified peptide was calculated based on the intensity information by the following steps: the intensities of modified peptides (I) were centralized and transformed into relative quantitative values (M) of modified peptides in each sample. The formula is listed as follows: i denotes the sample and j denotes the modified peptide. $Mij = Iij/Mean(Ij)$. The relative quantitative value of modified peptides corrected by median rate value of evidence intensity (N), as follows: $R_{ij} = M_{ij}/Median(N_j)$ to adjust the systematic bias of the modified peptides amount among different samples in the process of mass spectrometry detection. The relative quantitative value of the modified peptide is divided by the relative quantitative value of corresponding protein to remove the influence from protein expression of modifications.

Differential Analysis of Proteome and Phosphoproteome

For proteome differential analysis, the samples to be compared were selected in pairwise groups, and the fold change (FC) was then calculated by the ratio of the mean intensity for each protein in two sample groups. For example, to calculate the fold change between sample A and sample B, the formula is shown as following: R denotes the relative quantitative value of the protein, i denotes the sample, and k denotes the protein. $FC_{A/B,k} = Mean(R_{ik}, i \in A)/Mean(R_{ik}, i \in B)$. The student's t test was performed on the relative quantitative value of each to calculate the statistical significance of difference between groups. The relative quantitative value of proteins was applied with log2 transformation typically. The formula is shown as following: $P_{ik} = T.test(Log2(R_{ik}, i \in A), Log2(R_{ik}, i \in B))$.The protein with p value <0.05, the fold change >1.2 was regarded as significantly upregulated protein, while the protein with p value <0.05, the fold change <1/1.2 was regarded as significantly downregulated protein.

For phosphoproteome differential analysis, the samples to be compared were selected in pairwise, and the fold change was calculated as the ratio of the mean intensity for each modification site in two sample groups. The formula to calculate the fold change between sample A and sample B is listed as following: R denotes the relative quantitative value of the modification site, i denotes the sample, and k denotes the modification site. $FC_{A/B,k} = Mean(R_{ik}, i \in A)/Mean(R_{ik}, i \in B)$.Student's t test was performed on the relative quantitative value of each modification site in the two sample groups to calculate the significance of the difference between groups. The relative quantitative value of modification site was log2 transformed to make the data conform a normal distribution. The formula is listed as following: $P_{ik} = T.test(Log2(R_{ik}, i \in A), Log2(R_{ik}, i \in B))$.The modification site with p value <0.05, the fold change >1.2 was regarded as significant upregulated site, while the modification site with p value <0.05, the fold change <1/1.2 was regarded as significant downregulated site.

Motif Analysis

Soft motif x was used to analyze the model of sequences constituted with amino acids in specific positions to modify 21 mers (ten amino acids upstream and downstream of the site but phosphorylation with modify 13 mers that six amino acids upstream and downstream of 35/36 the site) in all protein sequences. All the database protein sequences were used as background database parameters, and other parameters were defaulted.

KEGG Pathway Annotation

The KEGG database was used to annotate protein pathways. First, the KEGG online service tool KAAS was used to annotate the protein KEGG database description. Then, the annotation result was mapped to the KEGG pathway database using the KEGG online service tool KEGG mapper.

RNA Isolation and cDNA Synthesis

Brain samples were homogenized in a homogenizer according to the protocol supplied with TransZol Reagent. The concentration of RNA was measured with spectrophotometry, and the reaction volume consisted of 1 μg of total RNA, 2× TS Reaction Mix, TransScript RT/RI Enzyme Mix (TransGen Biotech), oligo (dT), gDNA Remover, and RNase-free H_2O (to a final volume of 20 μl). The amplification program was as follows: 42 °C for 30 min, 85 °C for 5 s, and a final hold at 4 °C. cDNA synthesis was performed in a C1000 Touch Thermal Cycler (BIO-RAD).

Plasmids

The Syt1 open reading frame was PCR-amplified from C57BL/6J mouse hippocampal cDNA and subcloned into the NheI and BamHI sites of a pFUGW expression vector with PCR. $Syt1^{T112A}$ and $Syt1^{T112D}$ mutations were cloned into the NheI and BamHI sites of pFUGW using overlapping PCR. For GST pull down, the Syt1 CDS was PCR-amplified from the plasmid (pFUGW-Syt1) and subcloned into the BamHI and XhoI sites of a pGEX expression vector. For coimmunoprecipitation (Co-IP), the sequence of GFP-fusion-Syt1 was subcloned into the NheI and BamHI sites of a pFUGW expression vector with PCR. The coding sequence of FLAG (DYKDDDDK)-tagged Kcnq2 was PCR-amplified from C57BL/6J mouse hippocampal cDNA and subcloned into the BamHI and NheI sites of a pHT48 expression vector with PCR. $Kcnq2^{S52A}$ and $Kcnq2^{S52D}$ mutations were cloned into the BamHI and NheI sites of a pHT48 expression vector using overlapping PCR. Anxa6 was PCR-amplified from C57BL/6J mouse hippocampal cDNA and subcloned into the BamHI and XhoI sites of a pGEX expression vector with PCR. GFP-tagged Anxa6 and GFP-tagged truncated mutations were cloned into the BamHI and XhoI sites of a pCEP4 expression vector with PCR. PCR was performed with the following protocol on a MyCyclerTM Thermal Cycler (Bio–Rad): 98 °C for 90 s, 98 °C for 30 s, 55 °C for 30 s, 72 °C for 1 to 3 min (30 cycles); 72 °C for 5 min, and a final hold at 4 °C. The PCR products were analyzed on a 2% agarose gel. Primers are described in supplemental Table S3.

Primary Hippocampal Neurons and Calcium Phosphate Transfection

Cultured neurons were obtained from C57BL/6J mouse hippocampal cells, as described previously (14). Briefly, mouse hippocampal cells were dissected from postnatal day 0 WT mice, dissociated

with 0.25% trypsin (Gibco), digested for 12 min at 37 °C, plated on poly-D-lysine-coated glass coverslips (8 mm) at a density of 80,000 neurons per coverslip (Scope Cell Counter Basic), and maintained at 37 °C in 5% CO_2. Hippocampal neurons were transfected using the calcium-phosphate transfection method after 10 days of incubation (DIV 10) and analyzed on DIV 13 to 14, as described previously (14). Briefly, for each coverslip on a 48-well plate, 0.6 μg of the total plasmid was mixed with 0.99 μl of the 2 M $CaCl_2$ solution and ddH_2O to reach a final volume of 8 μl, and the DNA/$CaCl_2$ solution was added slowly to 8 μl of 2× HBS (631312, CalPhos Mammalian Transfection Kit, TaKaRa). The DNA/$CaCl_2$/HBS solution was incubated at room temperature for 30 min and then added to the neuronal cell cultures and incubated for 30 min in an incubator. The cells were washed once with medium containing $MgCl_2$ and were maintained in an incubator for 3 to 4 days (typically, 1% of neurons were transfected as assessed by counting GFP-positive neurons) before OGD and immunocytochemistry. Transfected neurons were chosen randomly, and images were acquired using a confocal microscope.

OGD

OGD experiments were performed using a specialized humidified chamber maintained at a constant temperature of 37 °C in an anaerobic atmosphere (90% N_2, 5% H_2, and 5% CO_2) (15) as described previously (8). Briefly, to initiate OGD, the culture medium was replaced with deoxygenated, glucose-free Dulbecco's modified Eagle's medium (DMEM, Life Technology, 11966025), the culture was treated for 2 h (OGD 2 h), and the culture medium was replaced with glucose-free DMEM plus glucose as a control.

HEK293T Cells and Transfection

Human embryonic kidney (HEK) 293T cells were grown at 37 °C supplied with 5% CO_2 in an incubator (Thermo Fisher) with a humidified atmosphere. The cells were grown in DMEM containing 10% fetal bovine serum. Cells were washed once using PBS and digested with 0.05% trypsin-EDTA (Gibco) at 37 °C for routine passage of the cells. All HEK293T cell transfections were performed using the PEI method. The PEI (1 mg/ml in ddH_2O): DNA ratio was 3:1. The PEI/DNA mixture was incubated for 30 min at room temperature before the mixture was added dropwise to the HEK293T cell cultures.

Brain Homogenate Preparations

Brain homogenate was prepared as described previously (8). One mouse hippocampus was homogenized in 1 ml of PBS, 1 mM PMSF, 1 μg/ml pepstatin, 1 μg/ml leupeptin, and 2 μg/ml aprotinin and adjusted to a final concentration of 1% Triton X-100 (T9284, Sigma). Proteins in the homogenate were extracted for 2 h at 4 °C, and insoluble debris was removed by centrifugation (0.5 h at 10,000*g*).

Western Blot

Protein extracts were denatured at 95 °C for 5 min and separated on 10% SDS–PAGE gels at 110 V for approximately 70 min. The proteins were transferred to nitrocellulose (NC, HATF00010, Millipore) filters at 80 V for 5 h. The NC membrane was initially blocked with 5% nonfat milk and 2% goat serum (16210064, Thermo Fisher(v/v)) in tris-buffered saline with 0.1% Tween 20 (93773, Sigma) at room temperature for 1 h. Monoclonal antibodies to β-actin (HC201-02, TransGen Biotech), polyclonal antibody to Syt1 (CSB-PA019553GA01HU, CUSABIO Biotech), rabbit polyclonal anti-phosphotyrosine (Cat# PTM-702, PTM BIO) were employed for Western blot analyses as primary antibodies at 4 °C overnight. After three washes of 5 min each with tris-buffered saline with 0.1% Tween 20, either goat anti-rabbit (HS101-01, TransGen Biotech) or anti-mouse (HS201-01, TransGen Biotech) immunoglobulin G was added at a dilution of 1:5000 as the secondary antibody. The NC membrane was scanned with an imaging system (MicroChemi 4.2, DNR Bio Imaging Systems).

Immunostaining

Cultures were fixed for 12 min with 4% paraformaldehyde and 4% sucrose in PBS (pH 7.4), followed by permeabilization with 0.2% Triton X-100 in PBS. An initial blocking step was performed with PBS containing 5% milk and 2% normal goat serum for 30 min (PBS-MILK/NGS) at room temperature, followed by incubation overnight with anti-Syt1 antibody or anti-MAP2 antibody diluted in PBS-MILK/NGS. After washing with PBS, cultures were incubated with Alexa Fluor 546-conjugated goat anti-rabbit antibody to detect Syt1 and MAP2. After washing with PBS, the samples were mounted with Fluoromount-G mounting medium (0100-01, Southern Biotechnology Associates, Inc). Stained neurons were chosen randomly, and images were acquired using a confocal microscope.

Administration of Tat-Syt1^{T112A} Peptides

Cultured hippocampal neurons were administered 10 μM Tat-V5 (Tat-GKPIPNPLLGLDST), Tat-Syt1^{WT} (Tat-KDVKDLGKTMKDQ), or Tat-Syt1^{T112A} (Tat-KDVKDLGKAMKDQ) 30 min before and during the control or OGD 2 h operation. Tat peptides (10 μM) were chosen because we found that they were not toxic to cells. FITC-labeled peptides with 99% purity were synthesized by Genscript Inc. For stereotactic injection of Tat-V5 or Tat-Syt1^{T112A}, glass pipettes were pulled from borosilicate glass capillary tubes (World Precision Instruments) using a P-97 micropipette puller (Sutter Instrument). Stereotactic injection (RWD 68526, RWD Life Science) of 2 μl (0.2 nM) of Tat-V5 or Tat-Syt1^{T112A} was injected through glass micropipettes and stopped at the injection site for 5 min. After 30 min of rest, the injected mice were subjected to sham or MCAO operation for 24 h.

LDH Release

OGD-induced cell injury was also quantified by measuring lactate dehydrogenase (LDH) release from damaged cells according to the manufacturer's instructions. In brief, 50 μl of LDH reaction reagent was added to 100 μl conditional medium taken from the cell culture wells. The absorbance was measured at 490 nm by a spectrophotometer plate reader. All values were normalized to the control group.

ATP Measurement

Intracellular ATP was determined by an ATP detection kit according to the manufacturer's instructions. In brief, 50 μl lysis buffer from an ATP detection kit was added to each well of a 48-well plate. The lysates were centrifuged at 12,000*g* for 5 min at 4 °C. Twenty microliters of supernatant were transferred to 100 μl of ATP reaction reagent in a 96-well plate. The absorbance was measured by a spectrophotometer plate reader. All values were normalized to the control group.

MTT Assay

Cell viability was measured with 3-(4,5-dimethylthiazol-2-yl)-2,5-diphenyltetrazolium bromide (MTT) assay according to the manufacturer's instructions. In brief, hippocampal neurons were seeded in 48-well plates (8×10^4 cells/well) and incubated for 14 days. The cultured neurons were incubated with 0.5 mg/ml MTT solution at 37 °C for 4 h, and the medium was carefully removed. Then, 100 μl of dimethylsulfoxide was added to each well to dissolve the violet formazan

crystals. The absorbance was measured at 570 nm by a spectrophotometer plate reader. All values were normalized to the control group.

Infarct Volume Evaluation

The size of the infarction was evaluated at 24 h after MCAO by using 2,3,5-tetrazolium chloride (TTC) staining as described previously (8). Briefly, mice were sacrificed under deep anesthesia at 24 h after MCAO. The brain was removed rapidly and cut into 2 mm thick coronal slices by a Mouse Brain Slicer (68707, RWD Life Science), and the slices were immersed in 2% TTC solution for 15 min at 37 °C. The size of the infarct volume was determined by examining the areas of TTC-stained slices that did not stain with TTC by using NIH ImageJ software.

Pulldown

WT Syt1 or Anxa6 was expressed as GST fusion proteins in pGEX-4T-1 and purified. For pulldowns from HEK293T cell lysates, cells were washed with PBS once, and the cell pellet was collected (20,000*g*, 1 min at 4 °C). Proteins were extracted from the cell pellet for 0.5 h at 4 °C in 50 mM Hepes–NaOH pH 7.4 containing 1% Triton, 1 mM EDTA, 2 mM $CaCl_2$, 1 mM $MgCl_2$, 50 mM KCl, and 100 mM NaCl with protease inhibitors (1 mM PMSF, 1 μg/ml pepstatin, 1 μg/ml leupeptin, and 2 μg/ml aprotinin). Insoluble material was removed by centrifugation (20,000*g* for 10 min), and the supernatant was used for various pulldowns. Prewashed 25 μl of GST beads was added and incubated overnight at 4 °C with gentle rotation. The GST beads were collected by centrifugation at 700*g* for 3 min at 4 °C. The beads were washed six times with ice-cold immunoprecipitation buffer (IPB, 50 mM Hepes, pH 7.4, 100 mM NaCl, 50 mM KCl, 2 mM $CaCl_2$, 2 mM $MgCl_2$, 1 mM EDTA, 1 μg/ml pepstatin, 1 μg/ml leupeptin, 2 μg/ml aprotinin, 1 mM PMSF, one tablet of protease inhibitor cocktail per 10 ml buffer) containing 0.1% Triton X-100. After the last wash, the beads were resuspended in 60 μl IPB buffer, and the pulled down proteins were eluted in 3× loading buffer and analyzed by Western blotting after boiling for 5 min at 100 °C.

Coimmunoprecipitation

CoIP was performed as previously described (16). Briefly, HEK293T cells transiently transfected with the indicated constructs in plates with a diameter of 10 cm were harvested at approximately 48 h posttransfection and centrifuged to remove the cell debris (20,000*g*, 10 min at 4 °C). Prewashed 20 μl of anti-GFP-Trap-A beads (Chromotek, gta-20) was added and incubated overnight at 4 °C with gentle rotation. The anti-GFP-Trap-A beads were collected by centrifugation at 1000*g* for 3 min at 4 °C. The beads were washed six times with ice-cold IPB (50 mM Hepes, pH 7.4, 100 mM NaCl, 50 mM KCl, 2 mM $CaCl_2$, 2 mM $MgCl_2$, 1 mM EDTA, 1 μg/ml pepstatin, 1 μg/ml leupeptin, 2 μg/ml aprotinin, 1 mM PMSF, one tablet of protease inhibitor cocktail per 10 ml buffer) containing 0.1% Triton X-100. After the last wash, the beads were resuspended in 60 μl IPB buffer, and the immunoprecipitated proteins were eluted in 3× loading buffer and analyzed by Western blotting after boiling for 5 min at 100 °C.

Data Quantification and Statistical Analyses

Replicates are defined as indicated in the figure legends. All analyses were performed using GraphPad Prism (V7.0) for Windows. Data are presented as the mean value ± SEM. For comparison of two groups, an unpaired Student's *t* test was performed (Figs. 2*B*, 3, *B*, *D*, *I*, and *K*, 4, *I* and *J*, 5*B* and 6, *C* and *F*). For comparison of more than two groups, one-way ANOVA tests followed by Tukey's multiple comparison tests were performed (Figs. 2, *D* and *G*, 3, *F* and *G*, 4, *D*–*G*, 5, *D* and *G*, 6, *H* and *J* and supplemental Fig. S7*D*). Changes were considered statistically significant when $p < 0.05$. The detailed *p* values for all statistical analysis are described in supplemental Table S4.

RESULTS

Global Hippocampal Phosphoproteome Reveals Synaptic Abnormalities in Acute Cerebral Ischemia

Posttranslational modifications (17) have been recognized as a common feature of proteins (17–19). To investigate the role of protein modification in the hippocampus after cerebral ischemia onset, phosphorylation of proteins was investigated by Western blot in hippocampal tissue lysates of sham and permanent focal cerebral ischemia rats by performing MCAO for various times (0.5 h, 1 h, 2 h, 3 h, 4 h, or 5 h). A marked elevation in phosphorylation was observed in cerebral ischemia 2 h mice relative to sham littermates (supplemental Fig. S1*A*), and equal amounts of loaded samples were verified by Coomassie blue staining (supplemental Fig. S1*B*). Furthermore, we detected phosphorylation in the cortex tissue lysates of sham and permanent focal cerebral ischemia 2 h. Consistent with the observations in hippocampus, an elevated level of phosphorylation was detected in cortex tissues of permanent focal cerebral ischemia 2 h relative to sham mice (supplemental Fig. S1, *C* and *D*). Next, to identify the phosphorylated sites of proteins in hippocampus during focal cerebral ischemia 2 h, we used multiplexed TMT and LC/LC–MS/MS approaches to quantify the phosphoproteome and proteome of hippocampal lysates from mice operated with sham or acute focal cerebral ischemia by MCAO for 2 h. As depicted in Figure 1*A*, hippocampus combined from either ten sham or ten focal cerebral ischemia 2 h mice were lysed, digested, labeled with different TMT tags, then pooled and analyzed by LC/LC–MS/MS (20). Five percent (40 μg) of the pool was used for whole proteome analysis, and the remaining 95% (760 μg) was subjected to phosphoproteome profiling. In total, we quantified 9062 phosphopeptides and 5174 proteins (supplemental Fig. S2, *A* and *B*, supplemental Table S1 and S2). Interestingly, 184 phosphorylation sites of 135 proteins were upregulated and 689 phosphorylation sites of 420 proteins were downregulated in the hippocampus 2 h after cerebral ischemia compared with sham operation (Fig. 1*B*). We utilized WoLFPSORT software to analyze the subcellular location of the dysregulated phosphorylated proteins and found that 50% of dysregulated phosphorylated proteins were localized to nucleus, 26% were cytoplasmic protein, another 16% were transported to plasma membranes, and the others were located to mitochondria (4%), extracellular (3%), and cytoskeleton (1%) (Fig. 1*C*), and the clustering analysis of dysregulated phosphorylated proteins were shown (Fig. 1*D* and supplemental Fig. S2, *F* and *G*). Moreover, 21 proteins were upregulated and seven proteins were downregulated in hippocampal lysates after cerebral ischemia for 2 h relative to sham lysates based on the fold change (supplemental Fig. S2*C*). Using WoLFPSORT software to analyze the

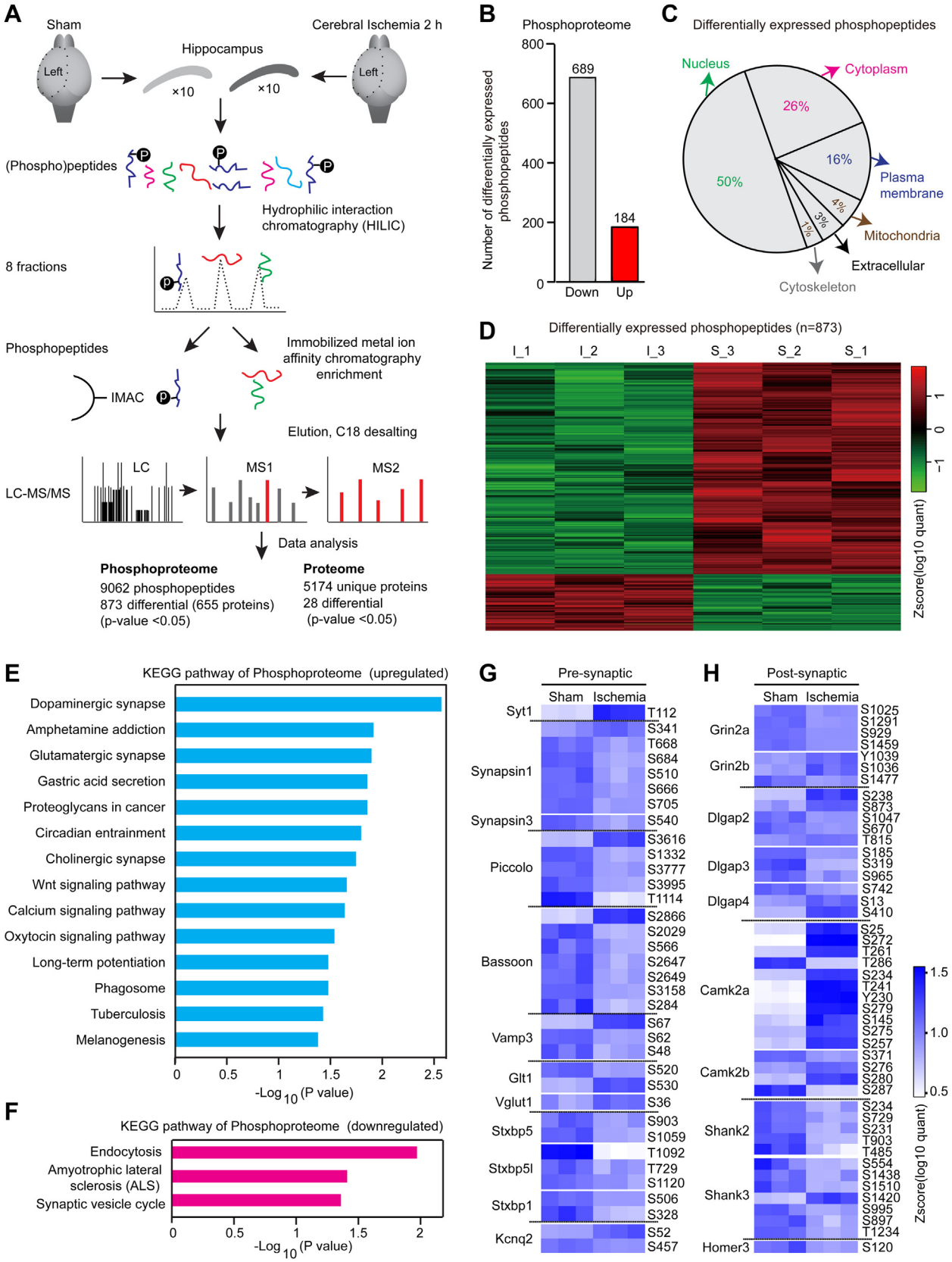

FIG. 1. **Global phosphoproteome of acute cerebral ischemic hippocampus reveals synaptic abnormalities.** *A*, schematic representation of the workflow used in this study. Pooled samples (ten hippocampi each after sham or acute MCAO ischemia for 2 h) were analyzed by three

subcellular location of dysregulated protein, 57% of detected dysregulated proteins were located to extracellular, 15% were cytoplasmic protein, another 11% were transport to nucleus, and the others were located to plasma membranes (10%), mitochondria (4%), and endoplasmic reticulum (3%) (supplemental Fig. S2*D*). Detailed clustering analysis of dysregulated proteins were shown (supplemental Fig. S2*E*). S100a9, alpha-2-HS-glycoprotein, fibrinogen beta chain, and complement component C3 (c3) were the most significantly changed, which was highly consistent with previous reports in cerebral ischemia injury (21–23). To better verify the validity of dysregulated proteins of the proteome, the PubMed database was employed for the search. We found that 14 proteins derived from proteomic profiling were in agreement with previously described functional results (21–29).

To further characterize the phosphoproteome and proteome of the hippocampus in acute cerebral ischemia, KEGG pathway analysis was performed for the dysregulated phosphorylated proteins. The data showed that phosphorylated proteins were enriched in dopaminergic synapses, amphetamine addiction, glutamatergic synapses (upregulated phosphorylation), endocytosis, amyotrophic lateral sclerosis, and the synaptic vesicle cycle (downregulated phosphorylation) (Fig. 1, *E* and *F*). Moreover, the phosphorylated proteins were enriched in PH-domain-like, PDZ, and calponin homology domains (supplemental Fig. S2*J*), which are often present in synaptic components and required for synaptic transmission (30–32). Interestingly, the phosphorylation of synaptic proteins such as Syt1, potassium voltage-gated channel subfamily KQT member 2 (Kcnq2), and postsynaptic calcium/calmodulin-dependent protein kinase type II subunit alpha, beta, and disks large-associated protein 2 was significantly changed, even though the function of those mediators in cerebral ischemia is still unclear (Fig. 1, *G* and *H*). These results indicated that the phosphorylation levels of certain proteins were rapidly altered upon acute cerebral ischemia compared to those in sham mouse. Next, motif analysis of the phosphoproteome showed that 85% were serine-type phosphorylated, approximately 14% were threonine-type phosphorylated, and 1% were tyrosine-type phosphorylated (supplemental Fig. S2, *H* and *I*). The KEGG pathway analysis of dysregulated proteins results showed that upregulated proteins were enriched in complement and coagulation cascades and platelet activation pathways (supplemental Fig. S2*K*), and downregulated proteins were enriched in systemic lupus erythematosus and alcoholism pathways (supplemental Fig. S2*L*). These data revealed synaptic abnormalities in acute cerebral ischemia.

Phosphorylation of Syt1 at the Thr112 Site Aggravates Primary Neuron Injury After OGD Treatment

Syt1 is anchored in vesicle membranes and mediates fast Ca^{2+}-dependent exocytosis of synaptic vesicles in hippocampal neurons (33). However, the function of Syt1 in cerebral ischemia is still unclear. The mass spectrometry data showed that the phosphorylation level of Syt1 at the Thr112 (T112) site was significantly upregulated in cerebral ischemia (Fig. 2, *A* and *B*). We next explored whether phosphorylation of Syt1 at the T112 site in cultured hippocampal neurons affects neuronal injury during OGD treatment. To test this idea, we generated WT, T112A-mutant lacking threonine phosphorylation site and T112D-mutant mimicking phosphorylate group and exhibiting constitutive phosphorylation status constructs of mouse Syt1 ($Syt1^{WT}$, $Syt1^{T112A}$, and $Syt1^{T112D}$) (supplemental Fig. S3*A*) and tested their effects on the cultured hippocampus neurons during OGD. We first transfected WT, T112A-mutant, and T112D-mutant constructs into HEK293T cells, and the fluorescence immunostaining data demonstrated that the WT, T112A-mutant, and T112D-mutant mouse Syt1 constructs were mainly localized at the cytoplasmic membrane (supplemental Fig. S3, *B* and *C*), suggesting that phosphorylation of Syt1 at the T112 site does not affect the trafficking of Syt1 to the membrane in HEK293T cells. We then cotransfected $Syt1^{WT}$, $Syt1^{T112A}$, or $Syt1^{T112D}$ with a GFP-encoding plasmid into cultured hippocampal neurons at 10 days *in vitro* (DIV) and performed OGD treatment at 14 DIV followed by examining the average length of dendrites in GFP-expressing cultured hippocampal neurons (Fig. 2*C* and supplemental Fig. S4*A*). We found that the overexpression of Syt1 in cultured hippocampal neurons significantly increased neuronal injury after OGD treatment compared to the control. Moreover, overexpressing $Syt1^{T112D}$ exhibiting constitutive phosphorylation at T112 of Syt1 significantly increased neuronal injury, while overexpressing the $Syt1^{T112A}$ mutant lacking phosphorylation at T112 of Syt1 significantly decreased neuronal injury (Fig. 2*D*). Next, we

MS runs. *B*, numbers of dysregulated phosphopeptides (based on fold changes in phosphorylation of >1.2 or <1/1.2, *t* test, *p* value < 0.05) from MCAO- and sham-operated hippocampi after 2 h. (sham: n = 3 repeat MS, MCAO: n = 3 repeat MS). *C*, the distribution of subcellular localization of dysregulated-expressed phosphopeptides from MCAO- and sham-operated hippocampi after 2 h. (sham: n = 3 repeat MS, MCAO: n = 3 repeat MS). *D*, cluster analysis of dysregulated phosphopeptides in the hippocampus of acute cerebral ischemia 2 h or sham mice. (sham: n = 3 repeat MS, MCAO: n = 3 repeat MS). *E*, KEGG pathway analysis of upregulated (based on fold changes in phosphorylation of >1.2, *t* test, *p* value < 0.05) phosphorylated proteins in the hippocampus after sham or acute cerebral ischemia for 2 h. (sham: n = 3 repeat MS, MCAO: n = 3 repeat MS). *F*, KEGG pathway analysis of downregulated (based on fold changes in phosphorylation of <1/1.2, *t* test, *p* value < 0.05) phosphorylated proteins in the hippocampus after sham or acute cerebral ischemia for 2 h. (sham: n = 3 repeat MS, MCAO: n = 3 repeat MS). *G* and *H*, the phosphorylated sites of dysregulated expressed presynaptic (*G*) and postsynaptic (*H*) phosphorylated proteins in the hippocampus 2 h after acute cerebral ischemia. (Sham: n = 3 repeat MS, MCAO: n = 3 repeat MS). KEGG, Kyoto Encyclopedia of Genes and Genomes; MCAO, middle cerebral artery occlusion.

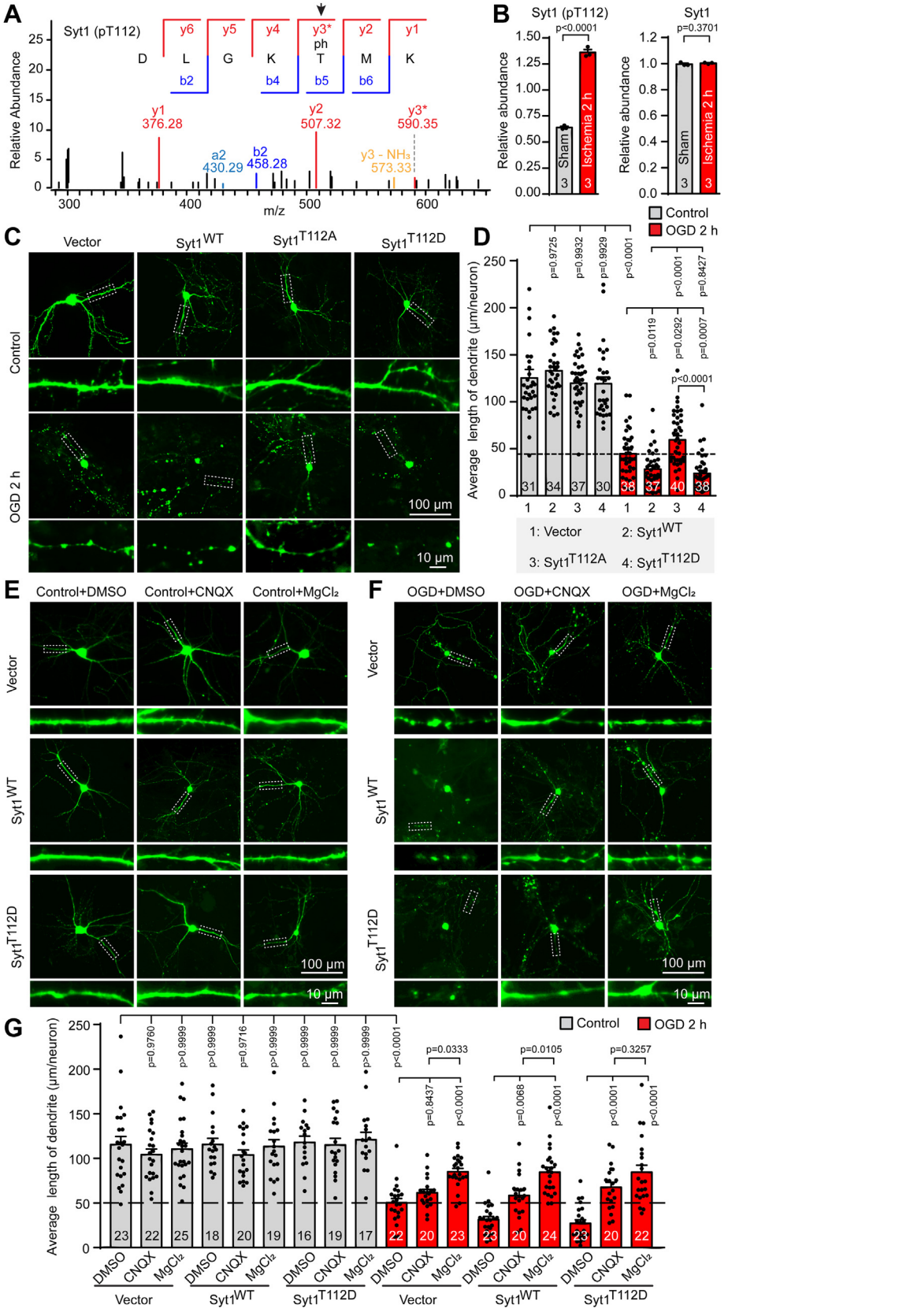
A
Syt1 (pT112)
y6 y5 y4 y3* y2 y1
D L G K ph T M K
b2 b4 b5 b6
y1 376.28
y2 507.32
y3* 590.35
a2 430.29
b2 458.28
y3 - NH3 573.33
Relative Abundance
m/z
B
Syt1 (pT112)
p<0.0001
Syt1
p=0.3701
Relative abundance
Sham
Ischemia 2 h
C
Vector
Syt1WT
Syt1T112A
Syt1T112D
Control
OGD 2 h
100 μm
10 μm
D
Control
OGD 2 h
Average length of dendrite (μm/neuron)
1: Vector
2: Syt1WT
3: Syt1T112A
4: Syt1T112D
E
Control+DMSO
Control+CNQX
Control+MgCl2
F
OGD+DMSO
OGD+CNQX
OGD+MgCl2
G
Control
OGD 2 h
Average length of dendrite (μm/neuron)
DMSO
CNQX
MgCl2
Vector
Syt1WT
Syt1T112D

used the antagonists CNQX and $MgCl_2$ to block α-amino-3-hydroxy-5-methyl-4-isoxazole-propionic acid and N-methyl-D-aspartic acid excitatory receptors, respectively, and then examined whether this phenomenon was restricted to excitatory receptors. We found that blocking excitatory α-amino-3-hydroxy-5-methyl-4-isoxazole-propionic acid or N-methyl-D-aspartic acid receptors significantly repressed $Syt1^{WT}$ overexpression or $Syt1^{T112D}$-mediated neuronal injury (Fig. 2, *E* and *F*). Taken together, these data demonstrate that phosphorylation of Syt1 at the T112 site in hippocampal neurons aggravates neuronal injury after acute cerebral ischemia.

Immature Neurons With Low Expression of Syt1 Exhibit Enhanced Tolerance to Cerebral Ischemia in Vitro *and* in Vivo

Since phosphorylation of Syt1 aggravates neuronal injury *via* excitatory receptors, we hypothesized that neurons with low expression of Syt1 could be more tolerant to cerebral ischemia injury. To test this idea, primary cultured hippocampal immature neurons were subjected to OGD treatment. Western blotting showed that the expression level of Syt1 in immature neurons (DIV.4) was lower than that in mature neurons (DIV.14) (Fig. 3, *A* and *B*). Consistently, the expression level of Syt1 in the hippocampus of immature mice (P14) was also lower than that of Syt1 in the hippocampus of mature mice (P56) (Fig. 3, *C* and *D*). Confocal imaging and quantification of MAP2 staining showed that immature neurons did not alter the structural morphology, while mature neurons significantly lost dendrites after OGD (Fig. 3, *E* and *F*). To further verify our observation, we also measured the relative level of LDH, which is released from damaged cells in the media (15) and reflects the viability of neurons after OGD treatment in conditioned medium. Consistent with morphological measures, LDH release in immature neurons was significantly lower than that in mature neurons after OGD *in vitro* (Fig. 3*G*). Next, we tested ischemia-induced infarct size in an MCAO model of immature and mature mice. The blood flow of both immature and mature mice detected by laser speckle imaging significantly decreased after cerebral ischemia onset (Fig. 3, *H* and *I*). Interestingly, the infarct size of ischemic brain slices after MCAO ischemia examined by using TTC staining in immature animals was significantly smaller than that in mature animals (Fig. 3, *J* and *K* and supplemental Fig. S4*B*). These results demonstrated that immature neurons with low expression of Syt1 exhibit enhanced tolerance to cerebral ischemia *in vitro* and *in vivo*, indicating that Syt1 plays a crucial role in acute cerebral ischemia-induced neuronal injury.

Tat-$Syt1^{T112A}$ Peptide Protects Neurons Against Cerebral Ischemia Neuron Injury

As the phosphorylation of Syt1 aggravates ischemic neuron injury in cultured neurons and neurons with low expression of Syt1 is tolerant to cerebral ischemia, we examined whether blocking the activity of Syt1 achieves therapeutic effects in a model of MCAO mice. To do so, we generated cell membrane-permeable $Syt1^{WT}$ and $Syt1^{T112A}$ peptides fusing $Syt1^{WT}$ and $Syt1^{T112A}$ to the cell membrane transduction domain of the HIV-1 Tat protein (9, 34) (Tat-$Syt1^{WT}$ and Tat-$Syt1^{T112A}$) (Fig. 4*A*). Immunostaining of Syt1 and tat-peptide showed that Tat-V5, Tat-$Syt1^{WT}$, and Tat-$Syt1^{T112A}$ colocalized with the presynaptic marker Syt1, suggesting that these peptides were transported to synapses (Fig. 4*B*). Next, we investigated the functional impacts of Tat peptide in hippocampal neurons following OGD treatment and found that Tat-$Syt1^{T112A}$, but not Tat-$Syt1^{WT}$, significantly decreased OGD-induced neuronal injury compared to the control (Fig. 4, *C*–*E*). To further examine the viability of neurons after Tat-peptide treatment, we also carried out ATP and MTT assays. Consistent with neuronal

FIG. 2. **Phosphorylation of Syt1 at Thr112 accelerates neuronal injury during OGD.** *A*, representative LC–MS/MS spectrum of phosphorylation of Syt1 at the threonine 112 (T112) site in the hippocampus 2 h after sham or acute MCAO ischemia. *B*, quantification of the phosphorylation level of Syt1 at the T112 site and the protein expression level of Syt1 2 h after ischemia. (sham: n = 3 repeat MS, MCAO: n = 3 repeat MS). *C*, representative images of hippocampal neurons transfected with pFUGW-GFP and either an empty vector (vector) or a plasmid encoding $Syt1^{WT}$, $Syt1^{T112A}$, or $Syt1^{T112D}$ at DIV 10 and subjected to control or OGD 2 h treatment at DIV 14. The scale bar represents 100 μm and 10 μm (magnified images). Transfected neurons were chosen randomly, and images were acquired using a confocal microscope. *D*, quantitative analysis of the average length of dendrites of neurons presented in (*C*). (control: vector: n = 31 cells/3 cultures, $Syt1^{WT}$: n = 34 cells/3 cultures, $Syt1^{T112A}$: n = 37 cells/3 cultures, $Syt1^{T112D}$: n = 30 cells/3 cultures; OGD 2 h: vector: n = 38 cells/3 cultures, $Syt1^{WT}$: n = 37 cells/3 cultures, $Syt1^{T112A}$: n = 40 cells/3 cultures, $Syt1^{T112D}$: n = 38 cells/3 cultures). *E* and *F*, representative images of hippocampal neurons transfected together with pFUGW-GFP and either an empty vector (control) or a plasmid encoding $Syt1^{WT}$ or $Syt1^{T112D}$ at DIV 10 and subjected to control (*E*) or OGD for 2 h (*F*) treatment at DIV 14 with DMSO, CNQX, or $MgCl_2$. The scale bar represents 100 μm and 10 μm (magnified images). Transfected neurons were chosen randomly, and images were acquired using a confocal microscope. *G*, quantitative analysis of the average length of dendrites of neurons presented in (*E*) and (*F*). (control: vector+DMSO: n = 23 cells/3 cultures, vector+CNQX: n = 22 cells/3 cultures, vector+$Mgcl_2$: n = 25 cells/3 cultures, $Syt1^{WT}$+DMSO: n = 18 cells/3 cultures, $Syt1^{WT}$+CNQX: n = 20 cells/3 cultures, $Syt1^{WT}$+$Mgcl_2$: n = 19 cells/3 cultures, $Syt1^{T112D}$+DMSO: n = 16 cells/3 cultures, $Syt1^{T112D}$+CNQX: n = 19 cells/3 cultures, $Syt1^{T112D}$+$Mgcl_2$: n = 17 cells/3 cultures; OGD 2 h: vector+DMSO: n = 22 cells/3 cultures, vector+CNQX: n = 20 cells/3 cultures, vector+$Mgcl_2$: n = 23 cells/3 cultures, $Syt1^{WT}$+DMSO: n = 23 cells/3 cultures, $Syt1^{WT}$+CNQX: n = 20 cells/3 cultures, $Syt1^{WT}$+Mgcl2: n = 24 cells/3 cultures, $Syt1^{T112D}$+DMSO: n = 23 cells/3 cultures, $Syt1^{T112D}$+CNQX: n = 20 cells/3 cultures, $Syt1^{T112D}$+Mgcl2: n = 22 cells/3 cultures). Data are presented as means ± SEM (error bars). The number of repeat times (*B*) and neurons (*D* and *G*) analyzed are indicated in columns. Unpaired Student's t tests (*B*) and one-way ANOVA tests followed by Tukey's multiple comparison tests (*D* and *G*) were performed. All experiments were repeated at least three times. DMSO, dimethylsulfoxide; MCAO, middle cerebral artery occlusion; OGD, oxygen-glucose deprivation.

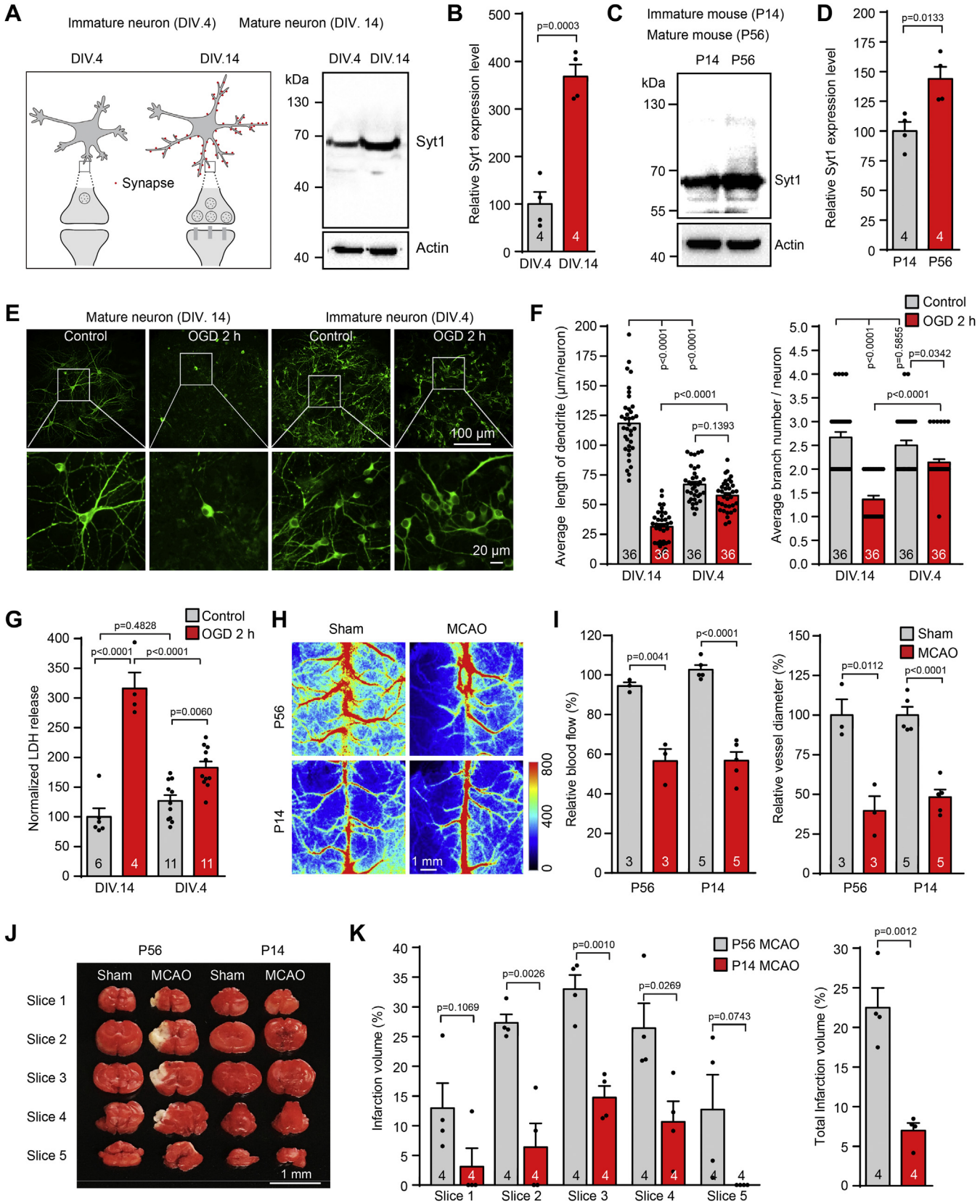

FIG. 3. **Immature neurons with low expression of Syt1 exhibit enhanced tolerance to cerebral ischemia *in vivo* and OGD *in vitro*.** *A* and *B*, representative Western blot image (*A*) and quantitative analysis (*B*) of the expression level of Syt1 in cultured immature and mature

morphological measurements, the relative intracellular ATP content and neuronal viability measured by MTT assay showed that Tat-Syt1^{T112A} significantly repressed neuronal injury resulting from OGD treatment (Fig. 4, *F* and *G*). To corroborate the neuroprotective effect of Tat-Syt1^{T112A} in an experimental ischemic stroke model, Tat-V5 or Tat-Syt1^{T112A} was stereotactically injected into the left brain followed by sham or MCAO operation. Using TTC staining to evaluate the infarct size of ischemic brain slices after MCAO (Fig. 4*H*), we found that the infarct volume ratio and neurological scores of the ischemic lesion in Tat-Syt1^{T112A}-injected mice were significantly smaller than those in Tat-V5-injected animals (Fig. 4, *I* and *J*). These results demonstrated a neuroprotective effect of Tat-Syt1^{T112A} in the experimental focal cerebral ischemia model. Collectively, our data suggested that the Tat-Syt1^{T112A} peptide protects neurons against cerebral ischemia injury.

Kcnq2 Interacts With Syt1 and Relieves Syt1-Mediated Neuronal Injury

The phosphoproteome data revealed that the phosphorylation level of Kcnq2 at the Ser52 (S52) site was significantly upregulated in cerebral ischemia (Fig. 5, *A* and *B*). To test the role of Kcnq2 phosphorylation at the S52 site, we created three constructs encoding WT, S52A-mutant lacking phosphorylation site, or S52D-mutant barbering constitutive phosphorylation status of mouse Kcnq2 (Kcnq2^{WT}, Kcnq2^{S52A}, and Kcnq2^{S52D}) (supplemental Fig. S5*A* in Supporting Information) and examined their effects in cultured hippocampal neurons with sham control or OGD treatment. First, we transfected WT, S52A-mutant, and S52D-mutant constructs into HEK293T cells followed by fluorescence immunostaining and verified that both S52A-mutant and S52D-mutant mouse Kcnq2 were localized to the cytoplasmic membrane as WT Kcnq2 was (supplemental Fig. S5, *B* and *C*), suggesting that phosphorylation of Kcnq2 at the S52 site does not affect the membrane trafficking of Kcnq2 in HEK293T cells. Next, we cotransfected plasmids encoding Kcnq2^{WT}, Kcnq2^{S52A}, and Kcnq2^{S52D} with GFP-encoding plasmids in cultured hippocampal neurons at DIV 10 and performed OGD treatment at DIV 14 followed by examining the structural morphology in GFP-expressing cultured hippocampal neurons. We found that the overexpression of Kcnq2 in cultured hippocampal neurons did not affect neuronal injury resulting from OGD treatment compared to the control. Furthermore, overexpressing either Kcnq2^{S52A} or Kcnq2^{S52D} did not affect neuronal injury resulting from OGD treatment (Fig. 5, *C* and *D*). Since previous studies determined that Kcnq2 interacts with Syntaxin1A (35) and Syntaxin1A interacts with Syt1 (36) and to ask if Kcnq2 binds directly with Syt1, we generated plasmids encoding Syt1 fused with glutathione-S-transferase (GST) or GST alone and expressed them in bacteria followed by purification to perform GST pull-down assays. We found that GST-Syt1 but not GST alone specifically pulled down Kcnq2 (supplemental Fig. S6*A*). To confirm these observations, we tested whether Syt1 fused with a GFP tag immunoprecipitated with Kcnq2 after overexpression in HKE293T cells and found that Syt1-GFP, but not GFP alone, interacted with Kcnq2 in CoIP experiments (Fig. 5*E*). To test whether Kcnq2 is involved in Syt1-mediated neuronal injury, plasmids encoding Kcnq2 and Syt1 were cotransfected into cultured mouse hippocampal neurons at DIV 10 and treated with OGD at DIV 14. Finally, confocal imaging and quantification of dendrite length were performed. We surprisingly found that Kcnq2 repressed Syt1-mediated neuronal injury induced by OGD treatment (Fig. 5, *F* and *G*). Taken together, these results suggested that Kcnq2 interacts with Syt1 and likely represses Syt1-mediated neuronal injury in cerebral ischemia.

Anxa6 Interacts With Kcnq2 and Protects Neurons Against Ischemia Injury

To further explore the molecular mechanism by which Kcnq2 represses Syt1-mediated neuronal injury upon OGD treatment, we predicted Kcnq2-interacting proteins by using the STRING database and found that the Ca^{2+}-dependent membrane-binding protein Anxa6 potentially interacts with

hippocampal neurons (immature neurons: n = 4 cultures, mature neurons, n = 4 cultures). *C* and *D*, representative Western blot image (*C*) and quantitative analysis (*D*) of the expression level of Syt1 in immature and mature mouse hippocampal tissue lysates (immature mice: n = 4 mice, mature mice, n = 4 mice). *E*, representative images of cultured mature and immature hippocampal neurons immunostained with an antibody against MAP2 after control or 2 h of OGD treatment. The scale bar represents 100 μm and 20 μm (magnified images). Stained neurons were chosen randomly, and images were acquired using a confocal microscope. *F*, quantitative analysis of the average length of MAP2 and branch number of neurons presented in (*E*) (Control: DIV 14: n = 36 cells/3 cultures, DIV 4: n = 36 cells/3 cultures; OGD 2 h: DIV 14: n = 36 cells/3 cultures, DIV 4: n = 36 cells/3 cultures). *G*, LDH release from cultured mature and immature hippocampal neurons after 2 h of control or 2 h of OGD treatment. (control: DIV 14: n = 6 wells/3 cultures, DIV 4: n = 11 wells/3 cultures; OGD 2 h: DIV 14: n = 4 wells/3 cultures, DIV 4: n = 11 wells/3 cultures). *H*, representative images of blood flow of mature and immature mice subjected to sham or MCAO operation for 24 h. *I*, quantitation of blood flow and vessel diameter of mature and immature mice after sham or MCAO operation for 24 h. (sham: immature mice: n = 5 mice, mature mice, n = 3 mice; MCAO 24 h: immature mice: n = 5 mice, mature mice, n = 3 mice). *J*, representative images of five coronal slices (2 mm each) of mature and immature mice subjected to sham or MCAO 24 h followed by staining with TTC. The scale bar represents 1 mm. *K*, quantitation of infarct size of slices 1 to 5 or total slices in (*K*) of mature and immature mice subjected to sham or MCAO operation for 24 h (MCAO 24 h: immature mice: n = 4 mice, mature mice, n = 4 mice). Data are presented as means ± SEM (error bars). The number of repeat times (*B* and *D*), neurons (*F*), wells (*G*), or mice (*I* and *K*) analyzed are indicated in columns. Unpaired Student's t tests (*B*, *D*, *I*, and *K*) and one-way ANOVA tests followed by Tukey's multiple comparison tests (*F* and *G*) were performed. All experiments were repeated at least three times. LDH, lactate dehydrogenase; MCAO, middle cerebral artery occlusion; OGD, oxygen-glucose deprivation; TTC, 2,3,5-tetrazolium chloride.

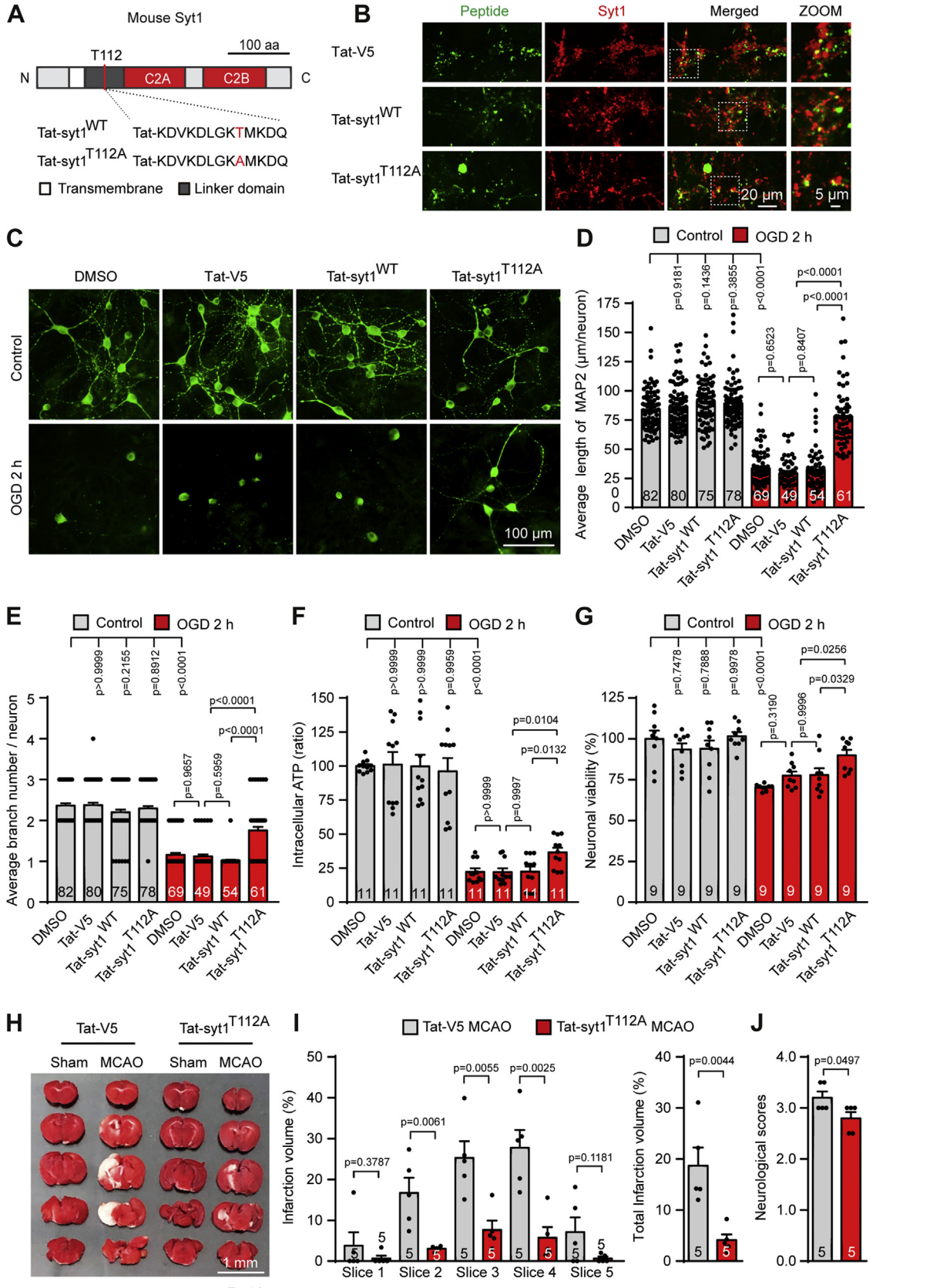

FIG. 4. **Administration of the Tat-Syt1^{T112A} peptide protects against neuronal injury in cerebral ischemia.** *A*, schematic diagram of mouse full-length Syt1 and tat peptides for Syt1^{WT} and Syt1^{T112A}. *B*, representative images of hippocampal neurons incubated with either Tat-V5

Kcnq2 (supplemental Fig. S6*B*). To identify this interaction, we expressed and purified Anxa6 fused with GST or GST alone (supplemental Fig. S6*C*) followed by GST pull-down assay with lysate of HEK293T cells expressing Kcnq2. We found that GST-Anxa6, but not GST alone, pulled down Kcnq2 from HEK293T cell lysates (Fig. 6*A*). Interestingly, the intensity of the Kcnq2 band pulled down by GST-Syt1, as examined by Western blotting, was dramatically decreased by the presence of EGTA, which chelates calcium in the solution (Fig. 6, *B* and *C*). We also expressed GFP tag-fused Anxa6 (Anxa6-GFP) or GFP alone with Flag-fused Kcnq2 (Kcnq2-Flag) in HEK293T cells and demonstrated that Anxa6 interacts with Kcnq2 in CoIP experiments (Fig. 6*D*). This interaction between Anxa6 and Kcnq2 observed in CoIP was Ca^{2+}-dependent (Fig. 6, *E* and *F*) and was consistent with the observations in the GST pull-down assay. To identify the binding region of Anxa6 interacting with Kcnq2, we created a series of GFP-fused Anxa6 N-terminal or C-terminal deletion mutants (supplemental Fig. S7). We first examined whether Anxa6 N-terminal or C-terminal deletion mutants affect Anxa6 subcellular localization in HEK293T cells by using confocal imaging and found that deletion of the first annexin repeat domain of Anxa6 did not alter Anxa6 localization, while other Anxa6 N-terminal or C-terminal deletion mutants obviously affected Anxa6 localization compared to WT in HEK293T cells (supplemental Fig. S7*B*). These data suggested that annexin repeat domains are required for Anxa6 trafficking to the cytoplasmic membrane. Furthermore, we also found that deletion of the C1-terminal domain of Anxa6 significantly increased its interaction with Kcnq2 compared to that of the WT (supplemental Fig. S7, *C* and *D*), indicating that the C1-terminal annexin repeat domain of Anxa6 antagonizes the interaction between Kcnq2 and Anxa6.

To determine whether Kcnq2 interaction with Anxa6 plays certain roles in the ischemia MCAO model or cultured hippocampal neurons with OGD treatment, we first transfected plasmids encoding Anxa6 into cultured hippocampal neurons followed by OGD treatment (Fig. 6, *G* and *H*) and found that overexpression of Anxa6 in cultured hippocampal neurons significantly decreased neuronal injury upon OGD treatment compared to the control. Second, we cotransfected plasmids encoding $Kcnq2^{WT}$ together with plasmids encoding Anxa6–GFP or GFP into cultured hippocampal neurons followed by OGD treatment, and we found that co-overexpression of Kcnq2 and Anxa6 in cultured hippocampal neurons showed a stronger protective effect on neuronal injury than that of control neurons or neurons overexpressing Anxa6 alone (Fig. 6, *G* and *H*). Taken together, these data indicate that the interaction of Kcnq2 with Anxa6 dependent on calcium promotes neuroprotection against neuronal injury in cerebral ischemia.

Since Kcnq2 interaction with Anxa6 alleviates neuronal injury during OGD, we therefore tested whether the Kcnq2/Anxa6 complex was sufficient to affect Syt1-mediated neuronal injury. We coexpressed Kcnq2 and Anxa6 in primary hippocampal neurons at DIV 10 and subjected them to OGD treatment at DIV 14 followed by confocal imaging and quantification of dendrite length and found that co-overexpression of Kcnq2 and Anxa6 nearly fully restored Syt1-mediated neuron injury upon OGD treatment (Fig. 6, *I* and *J*). Thus, these data support that the Kcnq2/Anxa6 complex alleviates Syt1-mediated neuronal injury in cerebral ischemia.

DISCUSSION

Phosphoproteome and Proteome After Acute Cerebral Ischemia

Significant effort has focused on the proteome and post-translational modification of proteins in cerebral ischemic stroke (37–41), but the phosphoproteome of neurons during cerebral ischemia has not been extensively examined. Considering that clinical intervention in the beginning few hours of cerebral ischemia onset is crucial for minimizing

(control), Tat-$Syt1^{WT}$, or Tat-$Syt1^{T112A}$, followed by double immunofluorescent staining with antibodies against Syt1 or Tat-peptide. The scale bar represents 20 μm and 5 μm (magnified images). *C*, representative images of hippocampal neurons incubated with DMSO, Tat-V5, Tat-$Syt1^{WT}$, or Tat-$Syt1^{T112A}$ followed by immunofluorescent staining with antibody against MAP2 after control or OGD treatment for 2 h. The scale bar represents 100 μm. Stained neurons were chosen randomly, and images were acquired using a confocal microscope. *D* and *E*, quantitative analysis of the average length (*D*) or the branch number (*E*) of neurons with positive MAP2 staining in (*C*). (control: DMSO: n = 82 cells/3 cultures, Tat-V5: n = 80 cells/3 cultures, Tat-$Syt1^{WT}$: n = 75 cells/3 cultures, Tat-$Syt1^{T112A}$: n = 78 cells/3 cultures; OGD 2 h: DMSO: n = 69 cells/3 cultures, Tat-V5: n = 49 cells/3 cultures, Tat-$Syt1^{WT}$: n = 54 cells/3 cultures, Tat-$Syt1^{T112A}$: n = 61 cells/3 cultures). *F* and *G*, quantitative analysis of the intracellular ATP content (*F*) and neuronal viability (*G*) of hippocampal neurons incubated with DMSO, Tat-V5, Tat-$Syt1^{WT}$, or Tat-$Syt1^{T112A}$ after control or OGD treatment for 2 h. (For ATP content, control: DMSO: n = 11 wells/3 cultures, Tat-V5: n = 11 wells/3 cultures, Tat-$Syt1^{WT}$: n = 11 wells/3 cultures, Tat-$Syt1^{T112A}$: n = 11 wells/3 cultures; OGD 2 h, DMSO: n = 11 wells/3 cultures, Tat-V5: n = 11 wells/3 cultures, Tat-$Syt1^{WT}$: n = 11 wells/3 cultures, Tat-$Syt1^{T112A}$: n = 11 wells/3 cultures. For neuronal viability, control: DMSO: n = 9 wells/3 cultures, Tat-V5: n = 9 wells/3 cultures, Tat-$Syt1^{WT}$: n = 9 wells/3 cultures, Tat-$Syt1^{T112A}$: n = 9 wells/3 cultures; OGD 2 h, DMSO: n = 9 wells/3 cultures, Tat-V5: n = 9 wells/3 cultures, Tat-$Syt1^{WT}$: n = 9 wells/3 cultures, Tat-$Syt1^{T112A}$: n = 9 wells/3 cultures). *H–J*, representative TTC staining images (*H*), infarct volume analysis (*I*), and neurological scores (*J*) of mice with stereotactic injection of Tat-V5 or Tat-$Syt1^{T112A}$ followed by sham or MCAO operation for 24 h. The scale bar represents 1 mm. (MCAO 24 h: Tat-V5: n = 5 mice: Tat-$Syt1^{T112A}$: n = 5 mice). Data are presented as means ± SEM (error bars). The number of neurons (*D* and *E*), wells (*F* and *G*), or mice (*I* and *J*) analyzed are indicated in columns. Unpaired Student's t tests (*I* and *J*) and one-way ANOVA tests followed by Tukey's multiple comparison tests (*D–G*) were performed. All experiments were repeated at least three times. DMSO, dimethylsulfoxide; MCAO, middle cerebral artery occlusion; OGD, oxygen-glucose deprivation; TTC, 2,3,5-tetrazolium chloride.

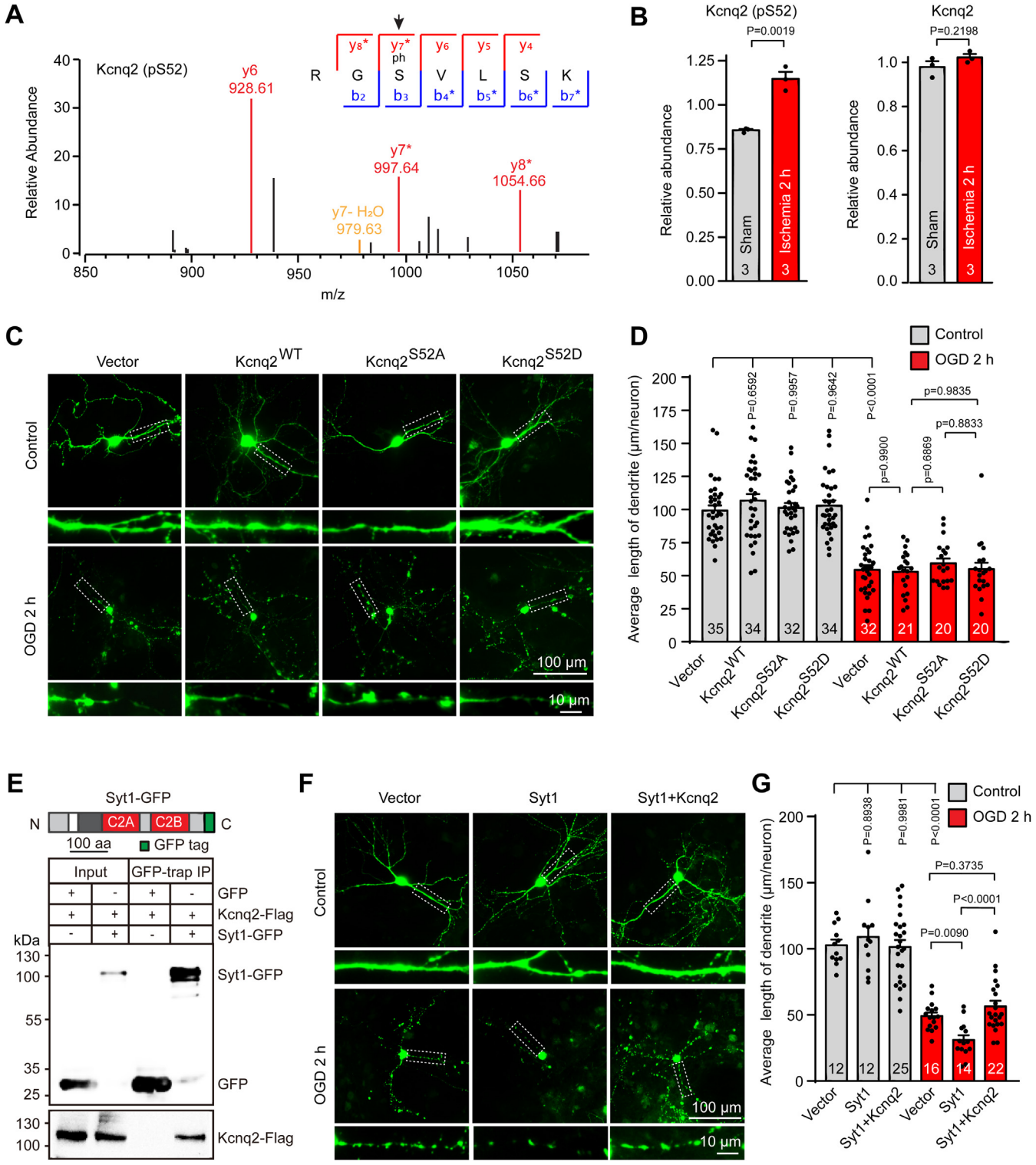

FIG. 5. **Kcnq2 interacts with Syt1 and alleviates Syt1-mediated neuronal injury by OGD treatment.** *A* and *B*, representative LC–MS/MS spectrum of Kcnq2 phosphorylation at the S52 site (*A*) and quantification of KCNQ phosphorylation at the S52 site and Kcnq2 protein expression level (*B*) in the hippocampus after sham or acute MCAO ischemia for 2 h. (sham: n = 3 repeat MS, MCAO: n = 3 repeat MS). *C* and *D*, representative images (*C*) and quantitative analysis (*D*) of the average length of dendrites of cultured hippocampal neurons transfected with pFUGW-GFP and either an empty vector or a plasmid encoding Kcnq2^{WT}, Kcnq2^{S52A}, or Kcnq2^{S52D} at DIV 10 followed by control or OGD treatment for 2 h at DIV 14. The scale bar represents 100 μm and 10 μm (magnified images). Transfected neurons were chosen randomly, and images were acquired using a confocal microscope. (control: vector: n = 35 cells/3 cultures, Kcnq2^{WT}: n = 34 cells/3 cultures, Kcnq2^{S52A}: n =

neuron injury and neuronal network damage and critical for brain functional and behavior recovery afterward (42), it is meaningful to investigate the global phosphoproteome of the acute cerebral ischemic brain to identify potential intervention targets for neuroprotection after acute cerebral ischemia onset. Here, we therefore established global phosphoproteome and proteome profiles of the acute cerebral ischemic hippocampus by using an MCAO model. Based on these integrated phosphoproteome and proteome profiles, we clarified some uncovered pathways in cerebral ischemia. For instance, we observed that regulating neurotransmission, synaptic structure, and excitatory receptors markedly increased phosphorylation in neurons in response to cerebral ischemia (Fig. 1), which is consistent with the potential explanation for excitotoxic glutamate efflux and build-up of intracellular calcium (33, 43, 44). Thus, the global phosphoproteome and proteome profiles and the dynamic changes in different pathways of acute cerebral ischemia in this study may provide a resource to understand the molecular pathology of acute cerebral ischemia.

Syt1 Phosphorylation Aggravates Neuronal Injury in Cerebral Ischemia

Syts comprise a family of synaptic vesicle proteins with at least 11 members, a couple of which are also present in nonneural cells (45–47). Syt1 and Syt2 are the most abundant isoforms expressed in neurons (48). Syt1 contains a short intravesicular domain, a single transmembrane region, a linker region followed by two large, conserved repeats of a sequence that is homologous to the regulatory region of Pkc mediating Ca^{2+}-dependent processes (C_2A and C_2B domains), and a short COOH-terminal region (49). Intravesicular N-glycosylation is essential for vesicular targeting of Syt1 (50). The R233Q mutation of Syt1 selectively impairs neurotransmitter release (51), and the F349A mutation selectively affects Syt1 oligomerization and eliminates Ca^{2+} control of exocytosis in PC12 cells (52). Previous studies suggest that CamkII and PkC phosphorylate the same residue, Thr112 (T112), in the linker region (53, 54). A mutation in Syt1 ($Syt1^{T112A}$) prevents its Pkc-dependent phosphorylation, which abolishes diacylglycerol-induced potentiation of synaptic transmission in hippocampal neurons (55). A recent study showed that a K^+ channel blocker rescued dominant-negative Syt1 mutant phenotypes in cultured neurons (56). However, the molecular machinery of Syt1 in cerebral ischemia remains elusive.

Here, we identified a member of the synaptic vesicle protein family required for neurotransmitter release, Syt1, whose phosphorylation level is induced by cerebral ischemia in an MCAO model and OGD treatment in primary hippocampal neurons. The phosphorylation of Syt1 at the T112 site aggravates a loss in the length of dendrites in primary hippocampal neurons upon OGD treatment (Fig. 2). The application of Tat-$Syt1^{T112A}$ peptides significantly protected neurons against injury in an ischemic stroke model (Fig. 4). Although the T112A-mutant and the T112D-mutant constructs of mouse Syt1 were employed in functional studies *in vitro*, it will be interesting to test T112A or T112D single site mutation knock-in animals to dissect the mechanism in cerebral ischemia.

Interestingly, we also observed that immature neurons with low expression of Syt1 were tolerant to OGD treatment *in vitro* and MCAO operation *in vivo* compared to mature neurons (Fig. 3). This complements previous observations in which blocking the excitatory transmission of neurons attenuates neuronal injury in a model of cerebral ischemia (7, 9, 57). Future work is needed to address the mechanism through comparative studies of the proteomes between immature neurons and mature neurons during OGD treatment.

Potassium Voltage-Gated Channel Kcnq2 Protects Neurons Against Ischemia Injury

Potassium voltage-gated channel Kcnq2 belongs to a family with five members, all of which have a membrane topology characteristic of the voltage-dependent K+ channel superfamily but possess large novel intracellular N- and C-termini (58). Kcnq2 is localized in several neuronal populations and underlies the M-current of hippocampal pyramidal cells (59–61). Mutations in Kcnq2 that disrupt the M-current cause excessive neuronal excitability (62). Several studies have determined that syntaxin1A (a plasma membrane protein component of the exocytotic SNARE complex) interacts physically and functionally with the cytoplasmic C-terminus of the K^+ channel (63–65). Mutations in the Kcnq2 gene encoding voltage-dependent K+ channel subunits cause neonatal

32 cells/3 cultures, $Kcnq2^{S52D}$: n = 34 cells/3 cultures; OGD 2 h: vector: n = 32 cells/3 cultures, $Kcnq2^{WT}$: n = 21 cells/3 cultures, $Kcnq2^{S52A}$: n = 20 cells/3 cultures, $Kcnq2^{S52D}$: n = 20 cells/3 cultures). *E*, coimmunoprecipitation of Flag-tagged Kcnq2 and GFP-tagged Syt1 (Syt1-GFP), or GFP alone, coexpressed in HEK293T cells. (n = 3 independent repeated experiment). *F* and *G*, representative images (*F*) and quantitative analysis (*G*) of the average length of dendrites of cultured hippocampal neurons transfected with pFUGW-GFP and a vector or a plasmid encoding Syt1 or plasmids encoding Syt1 or Kcnq2, respectively, at DIV 10 followed by control or OGD treatment for 2 h at DIV 14. The scale bar represents 100 μm and 10 μm (magnified images). Transfected neurons were chosen randomly, and images were acquired using a confocal microscope. (control: vector: n = 12 cells/3 cultures, Syt1: n = 12 cells/3 cultures, Syt1+ Kcnq2: n = 25 cells/3 cultures; OGD 2 h: vector: n = 16 cells/3 cultures, Syt1: n = 14 cells/3 cultures, Syt1+ Kcnq2: n = 22 cells/3 cultures). Data are presented as means ± SEM (error bars). The number of repeat times (*B*) and neurons (*D* and *G*) are indicated in columns. Unpaired Student's t tests (*B*) and one-way ANOVA tests followed by Tukey's multiple comparison tests (*D* and *G*) were performed. All experiments were repeated at least three times. HEK, human embryonic kidney; Kcnq2, potassium voltage-gated channel subfamily KQT member 2; MCAO, middle cerebral artery occlusion; OGD, oxygen-glucose deprivation.

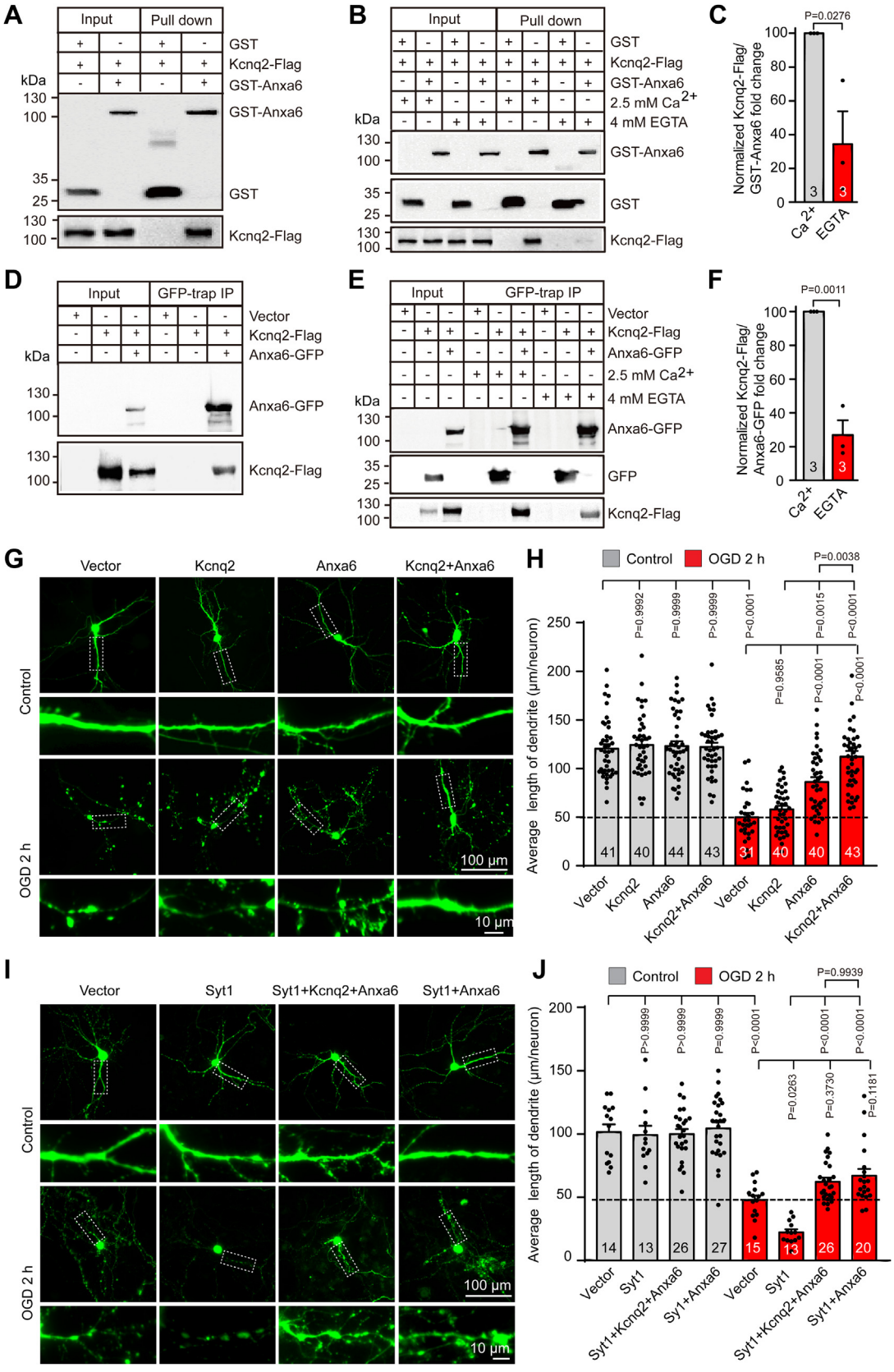

FIG. 6. **Kcnq2 interacts with Anxa6 and alleviates neuronal injury by inhibiting Syt1.** *A*, representative image of the glutathione-S-transferase (GST) pull-down assay of Flag-tagged Kcnq2 (Kcnq2-Flag) to immobilize GST fused to full-length Anxa6 or GST alone followed

epilepsies (66). However, the role of Kcnq2 in cerebral ischemia remains unclear.

Here, we identified that Kcnq2 interacts physically with Syt1 and that co-overexpression of Kcnq2 rescued Syt1-mediated neuronal injury during OGD (Fig. 5), whereas overexpression of Kcnq2 and Kcnq2^{S52A}-mutant and Kcnq2^{S52D}-mutant constructs failed to alleviate OGD-induced neuronal injury. This complements previous observations showing Syt1-associated neurodevelopmental disorder (56). Moreover, overexpression of Anxa6 alone in primary hippocampal neurons relieves neuronal injury. The Ca^{2+}-dependent interaction of Kcnq2 with Anxa6 significantly decreased neuronal injury during OGD. Co-overexpression of Kcnq2 and Anxa6 restored Syt1-mediated neuronal injury during OGD (Fig. 6). Our data suggest a model in which Kcnq2 binds Syt1 to relieve neuronal injury in cerebral ischemia. It is interesting to demonstrate the molecular and cellular mechanisms by which Kcnq2 alleviates ischemic neuron injury. For instance, which domains of Kcnq2 interact with Syt1 or Anxa6, we investigated whether phosphorylation of Kcnq2 at the S52 site or Syt1 at the T112 site influences these interactions.

Membrane-Binding Proteins Anxa6 and Kcnq2 Form a Complex to Relieve Syt1-Mediated Neuronal Injury

Anxa6 belongs to a conserved family of Ca^{2+}-dependent membrane-binding proteins. Previous studies revealed that Anxa6 is linked to its ability to bind phospholipids in cellular membranes in a dynamic and reversible fashion, particularly during the regulation of exocytic and endocytic pathways (67, 68). Anxa6 is expressed in hippocampal pyramidal cells (69) and binds to the head domain of synapsin1. The phosphorylation of synapsin1 by Ca^{2+}/calmodulin-dependent protein kinase II or cyclic AMP-dependent protein kinase prevents Anxa6 binding (70). A previous study showed that hypoxia promotes the interaction of Anxa6 with the plasma membrane (71). However, the role of Anxa6 in cerebral ischemia remains to be investigated. In this study, we found that the interaction of Kcnq2 with Anxa6 is dependent on calcium and may prevent the activity of Syt1, decrease excitatory neurotransmission at synapses, and promote neuroprotection against neuronal injury in cerebral ischemia.

A strength of our study is the description of the *in vivo* neuronal phosphoproteome during cerebral ischemia in a mouse model. However, to carry out such phosphoproteome profiling, total hippocampal tissue lysates were used to retrieve proteins that include dentate granule neurons and pyramidal neurons of the cornu ammonis area CA1–CA3, and other types of brain cells, such as astrocytes and microglia, may influence the neuronal phosphoproteome. In the future, using a targeted extraction method and specific chromatography column would probably increase the special neuron coverage. In addition, the datasets here were derived from 2 h after cerebral ischemia onset, and phosphoproteome profiling of neurons during cerebral ischemia for various times would probably provide dynamic presynaptic and postsynaptic modifications. Although single-cell proteome analysis is still in its infancy, such an emerging technology is a promising tool to profile the proteome during cerebral ischemia.

In summary, we explored the profiles of the phosphoproteome and proteome and characterized phosphoproteomic patterns during cerebral ischemia. Our dataset constructs a framework for future studies to address the complex interplay between presynaptics and postsynaptics in cerebral ischemic stroke. Additionally, these findings may provide tremendous opportunities to understand the mechanisms underlying neuronal injury during cerebral ischemia and potential targets for neuroprotection interventions.

by Western blotting. (n = 3 independent repeated experiment). *B* and *C*, representative image (*B*) and quantitation (*C*) of the GST pull assay of Kcnq2-Flag proteins bound to GST-Anxa6 or GST in the presence of 2.5 mM Ca^{2+} or 4 mM EGTA, respectively, followed by Western blotting. (n = 3 independent repeated experiment). *D*, representative image of coimmunoprecipitation showing that Kcnq2-Flag was immunoprecipitated by GFP-tagged Anxa6 (Anxa6-GFP) in HEK293T cells. (n = 3 independent repeated experiment). *E* and *F*, representative image (*E*) and quantification (*F*) of coimmunoprecipitation of Kcnq2-Flag with Anxa6-GFP or GFP alone in the presence of 2.5 mM Ca^{2+} or 4 mM EGTA, respectively, followed by Western blotting. (n = 3 independent repeated experiment). *G* and *H*, representative images (*G*) and quantitative analysis of the average length of dendrites (*H*) of hippocampal neurons transfected with pFUGW-GFP and a vector, a plasmid encoding Kcnq2, or Anxa6, or plasmids encoding Kcnq2 or Anxa6 together at DIV 10 followed by control or OGD treatment for 2 h at DIV 14. Transfected neurons were chosen randomly, and images were acquired using a confocal microscope. (control: vector: n = 41 cells/3 cultures, Kcnq2: n = 40 cells/3 cultures, Anxa6: n = 44 cells/3 cultures, Kcnq2+Anxa6: n = 43 cells/3 cultures; OGD 2 h: vector: n = 31 cells/3 cultures, Kcnq2: n = 40 cells/3 cultures, Anxa6: n = 40 cells/3 cultures, Kcnq2+Anxa6: n = 43 cells/3 cultures). *I* and *J*, representative images (*I*) and quantitative analysis of the average length of dendrites (*J*) of cultured hippocampal neurons transfected with pFUGW-GFP and a vector or a plasmid encoding Syt1, or plasmids encoding Syt1, Kcnq2, and Anxa6, respectively, together at DIV 10 followed by control or OGD treatment for 2 h at DIV 14. The scale bar represents 100 μm and 10 μm (magnified images). Transfected neurons were chosen randomly, and images were acquired using a confocal microscope. (control: vector: n = 14 cells/3 cultures, Syt1: n = 13 cells/3 cultures, Syt1+ Kcnq2+Anxa6: n = 26 cells/3 cultures, Syt1+Anxa6: n = 27 cells/3 cultures; OGD 2 h: vector: n = 15 cells/3 cultures, Syt1: n = 13 cells/3 cultures, Syt1+ Kcnq2+Anxa6: n = 26 cells/3 cultures, Syt1+Anxa6: n = 20 cells/3 cultures). Data are presented as means ± SEM (error bars). The number of repeat times (*C* and *F*) and neurons (*H* and *J*) analyzed are indicated in columns. Unpaired Student's t tests (*C* and *F*) and one-way ANOVA tests followed by Tukey's multiple comparison tests (*H* and *J*) were performed. All experiments were repeated at least three times. Anxa6, Annexin A6; Kcnq2, potassium voltage-gated channel subfamily KQT member 2; OGD, oxygen-glucose deprivation.

DATA AVAILABILITY

The mass spectrometry proteomics and phosphoproteomics data have been deposited to the ProteomeXchange Consortium *via* the PRIDE partner repository with the dataset identifier PXD027145.

Supplemental data—This article contains supplemental data.

Acknowledgments—This work was supported by National Key Research and Development Program of China (2021YFA090164), Hunan Provincial Key Research and Development Project (2020SK2092), and the Free Exploration Foundation of Shenzhen Science and Technology Innovation Committee (JCYJ20210324121000001).

Funding and additional information—This work was supported by the Provincial Natural Science Foundation of Hunan Province (Grant 2021JJ30098 to H. T. and Grant 2021JJ40053 to W. J.).

Author contributions—W. J., P. Y., N. K., and H. T. conceptualization; W. J., P. Y., N. K., and H. T. methodology; W. J., P. Z., P. Y., N. K., J. L., and Y. A. investigation; W. J. and P. Y. formal analysis; W. J. and H. T. writing–original draft; W. J., P. Z., P. Y., N. K., J. L., Y. A., and H. T. writing–review and editing.

Conflict of interest—The authors declare no competing interests.

Abbreviations—The abbreviations used are: Anxa6, Annexin A6; CoIP, coimmunoprecipitation; ECA, external carotid artery; FC, fold change; HEK, human embryonic kidney; IMAC, immobilized metal-ion affinity chromatography; IPB, immunoprecipitation buffer; Kcnq2, potassium voltage-gated channel subfamily KQT member 2; KEGG, Kyoto Encyclopedia of Genes and Genomes; LDH, lactate dehydrogenase; MCAO, middle cerebral artery occlusion; MS/MS, tandem mass spectrometry; MTT, 3-(4,5-dimethylthiazol-2-yl)-2,5-diphenyltetrazolium bromide; NC, nitrocellulose; OGD, oxygen-glucose deprivation; TMT, tandem mass tag; TTC, 2,3,5-tetrazolium chloride.

Received January 5, 2022, and in revised from, February 23, 2022
Published, MCPRO Papers in Press, March 5, 2022, https://doi.org/10.1016/j.mcpro.2022.100222

REFERENCES

1. Zhang, L., Zhang, R. L., Jiang, Q., Ding, G., Chopp, M., and Zhang, Z. G. (2015) Focal embolic cerebral ischemia in the rat. *Nat. Protoc.* **10**, 539–547
2. Lo, E. H., Dalkara, T., and Moskowitz, M. A. (2003) Mechanisms, challenges and opportunities in stroke. *Nat. Rev. Neurosci.* **4**, 399–415
3. Frese, C. K., Mikhaylova, M., Stucchi, R., Gautier, V., Liu, Q., Mohammed, S., Heck, A. J. R., Altelaar, A. F. M., and Hoogenraad, C. C. (2017) Quantitative map of proteome dynamics during neuronal differentiation. *Cell Rep.* **18**, 1527–1542
4. Hekman, R. M., Hume, A. J., Goel, R. K., Abo, K. M., Huang, J., Blum, B. C., Werder, R. B., Suder, E. L., Paul, I., Phanse, S., Youssef, A., Alysandratos, K. D., Padhorny, D., Ojha, S., Mora-Martin, A., *et al*. (2020) Actionable cytopathogenic host responses of human alveolar type 2 cells to SARS-CoV-2. *Mol. Cell* **80**, 1104–1122.e9
5. Li, L., Zhu, S., Shu, W., Guo, Y., Guan, Y., Zeng, J., Wang, H., Han, L., Zhang, J., Liu, X., Li, C., Hou, X., Gao, M., Ge, J., Ren, C., *et al*. (2020) Characterization of metabolic patterns in mouse oocytes during meiotic maturation. *Mol. Cell* **80**, 525–540.e9
6. Nakamura, K., Kustatscher, G., Alabert, C., Hodl, M., Forne, I., Volker-Albert, M., Satpathy, S., Beyer, T. E., Mailand, N., Choudhary, C., Imhof, A., Rappsilber, J., and Groth, A. (2021) Proteome dynamics at broken replication forks reveal a distinct ATM-directed repair response suppressing DNA double-strand break ubiquitination. *Mol. Cell* **81**, 1084–1099.e6
7. Wang, J., Liu, S., Fu, Y., Wang, J. H., and Lu, Y. (2003) Cdk5 activation induces hippocampal CA1 cell death by directly phosphorylating NMDA receptors. *Nat. Neurosci.* **6**, 1039–1047
8. Jiang, W., Tian, X., Yang, P., Li, J., Xiao, L., Liu, J., Liu, C., Tan, W., and Tu, H. (2019) Enolase1 alleviates cerebral ischemia-induced neuronal injury via its enzymatic product phosphoenolpyruvate. *ACS Chem. Neurosci.* **10**, 2877–2889
9. Tu, W., Xu, X., Peng, L., Zhong, X., Zhang, W., Soundarapandian, M. M., Balel, C., Wang, M., Jia, N., Zhang, W., Lew, F., Chan, S. L., Chen, Y., and Lu, Y. (2010) DAPK1 interaction with NMDA receptor NR2B subunits mediates brain damage in stroke. *Cell* **140**, 222–234
10. Wen, M., Jin, Y., Zhang, H., Sun, X., Kuai, Y., and Tan, W. (2019) Proteomic analysis of rat cerebral cortex in the subacute to long-term phases of focal cerebral ischemia-reperfusion injury. *J. Proteome Res.* **18**, 3099–3118
11. Lowenthal, M. S., Markey, S. P., and Dosemeci, A. (2015) Quantitative mass spectrometry measurements reveal stoichiometry of principal postsynaptic density proteins. *J. Proteome Res.* **14**, 2528–2538
12. Hyakkoku, K., Hamanaka, J., Tsuruma, K., Shimazawa, M., and Hara, H. (2010) Proteomic approach with LCMS-IT-TOF identified an increase of Rab33B after transient focal cerebral ischemia in mice. *Exp. Transl. Stroke Med.* **2**, 20
13. Uluc, K., Miranpuri, A., Kujoth, G. C., Akture, E., and Baskaya, M. K. (2011) Focal cerebral ischemia model by endovascular suture occlusion of the middle cerebral artery in the rat. *J. Vis. Exp.* https://doi.org/10.3791/1978
14. Jiang, W., Wei, M., Liu, M., Pan, Y., Cao, D., Yang, X., and Zhang, C. (2017) Identification of protein tyrosine phosphatase receptor type O (PTPRO) as a synaptic adhesion molecule that promotes synapse formation. *J. Neurosci.* **37**, 9828–9843
15. Hayakawa, K., Esposito, E., Wang, X., Terasaki, Y., Liu, Y., Xing, C., Ji, X., and Lo, E. H. (2016) Transfer of mitochondria from astrocytes to neurons after stroke. *Nature* **535**, 551–555
16. Zheng, Z., Zhang, X., Liu, J., He, P., Zhang, S., Zhang, Y., Gao, J., Yang, S., Kang, N., Afridi, M. I., Gao, S., Chen, C., and Tu, H. (2021) GABAergic synapses suppress intestinal innate immunity via insulin signaling in Caenorhabditis elegans. *Proc. Natl. Acad. Sci. U. S. A.* **118**, e2021063118
17. Nussinov, R., Tsai, C. J., Xin, F., and Radivojac, P. (2012) Allosteric post-translational modification codes. *Trends Biochem. Sci.* **37**, 447–455
18. Strahl, B. D., and Allis, C. D. (2000) The language of covalent histone modifications. *Nature* **403**, 41–45
19. Walsh, C. T., Garneau-Tsodikova, S., and Gatto, G. J., Jr. (2005) Protein posttranslational modifications: The chemistry of proteome diversifications. *Angew. Chem. Int. Ed. Engl.* **44**, 7342–7372
20. Wang, H., Yang, Y., Li, Y., Bai, B., Wang, X., Tan, H., Liu, T., Beach, T. G., Peng, J., and Wu, Z. (2015) Systematic optimization of long gradient chromatography mass spectrometry for deep analysis of brain proteome. *J. Proteome Res.* **14**, 829–838
21. Ziegler, G., Prinz, V., Albrecht, M. W., Harhausen, D., Khojasteh, U., Nacken, W., Endres, M., Dirnagl, U., Nietfeld, W., and Trendelenburg, G. (2009) Mrp-8 and -14 mediate CNS injury in focal cerebral ischemia. *Biochim. Biophys. Acta* **1792**, 1198–1204
22. Wang, H., Li, W., Zhu, S., Li, J., D'Amore, J., Ward, M. F., Yang, H., Wu, R., Jahnen-Dechent, W., Tracey, K. J., Wang, P., and Sama, A. E. (2010) Peripheral administration of fetuin-A attenuates early cerebral ischemic injury in rats. *J. Cereb. Blood Flow Metab.* **30**, 493–504
23. Lin, Z., Lin, H., Li, W., Huang, Y., and Dai, H. (2018) Complement component C3 promotes cerebral ischemia/reperfusion injury mediated by

TLR2/NFkappaB activation in diabetic mice. *Neurochem. Res.* **43**, 1599–1607
24. Cabezas-Llobet, N., Camprubi, S., Garcia, B., Alberch, J., and Xifro, X. (2018) Human alpha 1-antitrypsin protects neurons and glial cells against oxygen and glucose deprivation through inhibition of interleukins expression. *Biochim. Biophys. Acta Gen. Subj.* **1862**, 1852–1861
25. Debette, S., Kamatani, Y., Metso, T. M., Kloss, M., Chauhan, G., Engelter, S. T., Pezzini, A., Thijs, V., Markus, H. S., Dichgans, M., Wolf, C., Dittrich, R., Touze, E., Southerland, A. M., Samson, Y., *et al*. (2015) Common variation in PHACTR1 is associated with susceptibility to cervical artery dissection. *Nat. Genet.* **47**, 78–83
26. Dong, B., Zhang, Z., Xie, K., Yang, Y., Shi, Y., Wang, C., and Yu, Y. (2018) Hemopexin promotes angiogenesis via up-regulating HO-1 in rats after cerebral ischemia-reperfusion injury. *BMC Anesthesiol.* **18**, 2
27. Iwakuma, M., Anzai, T., Kobayashi, S., Ogata, M., Kaneda, Y., Ohno, K., and Saji, M. (2003) Antisense *in vivo* knockdown of synaptotagmin I and synapsin I by HVJ-liposome mediated gene transfer modulates ischemic injury of hippocampus in opposing ways. *Neurosci. Res.* **45**, 285–296
28. Salas, M. A., Valverde, C. A., Sanchez, G., Said, M., Rodriguez, J. S., Portiansky, E. L., Kaetzel, M. A., Dedman, J. R., Donoso, P., Kranias, E. G., and Mattiazzi, A. (2010) The signalling pathway of CaMKII-mediated apoptosis and necrosis in the ischemia/reperfusion injury. *J. Mol. Cell. Cardiol.* **48**, 1298–1306
29. Tian, X., Gotoh, T., Tsuji, K., Lo, E. H., Huang, S., and Feig, L. A. (2004) Developmentally regulated role for Ras-GRFs in coupling NMDA glutamate receptors to Ras, Erk and CREB. *EMBO J.* **23**, 1567–1575
30. Rao, S., Kay, Y., and Herring, B. E. (2019) Tiam1 is critical for glutamatergic synapse structure and function in the Hippocampus. *J. Neurosci.* **39**, 9306–9315
31. Ponna, S. K., Ruskamo, S., Myllykoski, M., Keller, C., Boeckers, T. M., and Kursula, P. (2018) Structural basis for PDZ domain interactions in the post-synaptic density scaffolding protein Shank3. *J. Neurochem.* **145**, 449–463
32. Zeng, M., Shang, Y., Guo, T., He, Q., Yung, W. H., Liu, K., and Zhang, M. (2016) A binding site outside the canonical PDZ domain determines the specific interaction between Shank and SAPAP and their function. *Proc. Natl. Acad. Sci. U. S. A.* **113**, E3081–E3090
33. Geppert, M., Goda, Y., Hammer, R. E., Li, C., Rosahl, T. W., Stevens, C. F., and Sudhof, T. C. (1994) Synaptotagmin I: A major Ca2+ sensor for transmitter release at a central synapse. *Cell* **79**, 717–727
34. Vives, E., Brodin, P., and Lebleu, B. (1997) A truncated HIV-1 Tat protein basic domain rapidly translocates through the plasma membrane and accumulates in the cell nucleus. *J. Biol. Chem.* **272**, 16010–16017
35. Etzioni, A., Siloni, S., Chikvashvilli, D., Strulovich, R., Sachyani, D., Regev, N., Greitzer-Antes, D., Hirsch, J. A., and Lotan, I. (2011) Regulation of neuronal M-channel gating in an isoform-specific manner: Functional interplay between calmodulin and syntaxin 1A. *J. Neurosci.* **31**, 14158–14171
36. Masumoto, T., Suzuki, K., Ohmori, I., Michiue, H., Tomizawa, K., Fujimura, A., Nishiki, T., and Matsui, H. (2012) Ca(2+)-independent syntaxin binding to the C(2)B effector region of synaptotagmin. *Mol. Cell. Neurosci.* **49**, 1–8
37. Datta, A., Jingru, Q., Khor, T. H., Teo, M. T., Heese, K., and Sze, S. K. (2011) Quantitative neuroproteomics of an *in vivo* rodent model of focal cerebral ischemia/reperfusion injury reveals a temporal regulation of novel pathophysiological molecular markers. *J. Proteome Res.* **10**, 5199–5213
38. Hu, B. R., Martone, M. E., Jones, Y. Z., and Liu, C. L. (2000) Protein aggregation after transient cerebral ischemia. *J. Neurosci.* **20**, 3191–3199
39. Hu, B. R., Janelidze, S., Ginsberg, M. D., Busto, R., Perez-Pinzon, M., Sick, T. J., Siesjo, B. K., and Liu, C. L. (2001) Protein aggregation after focal brain ischemia and reperfusion. *J. Cereb. Blood Flow Metab.* **21**, 865–875
40. Gu, R. F., Fang, T., Nelson, A., Gyoneva, S., Gao, B., Hedde, J., Henry, K., Peterson, E., Burkly, L. C., and Wei, R. (2021) Proteomic characterization of the dynamics of ischemic stroke in mice. *J. Proteome Res.* **20**, 3689–3700
41. Yang, W., Sheng, H., Thompson, J. W., Zhao, S., Wang, L., Miao, P., Liu, X., Moseley, M. A., and Paschen, W. (2014) Small ubiquitin-like modifier 3-modified proteome regulated by brain ischemia in novel small ubiquitin-like modifier transgenic mice: Putative protective proteins/pathways. *Stroke* **45**, 1115–1122
42. Murphy, T. H., and Corbett, D. (2009) Plasticity during stroke recovery: From synapse to behaviour. *Nat. Rev. Neurosci.* **10**, 861–872
43. Madden, D. R. (2002) The structure and function of glutamate receptor ion channels. *Nat. Rev. Neurosci.* **3**, 91–101
44. Monteiro, P., and Feng, G. (2017) SHANK proteins: Roles at the synapse and in autism spectrum disorder. *Nat. Rev. Neurosci.* **18**, 147–157
45. Sudhof, T. C., and Rizo, J. (1996) Synaptotagmins: C2-domain proteins that regulate membrane traffic. *Neuron* **17**, 379–388
46. Babity, J. M., Armstrong, J. N., Plumier, J. C., Currie, R. W., and Robertson, H. A. (1997) A novel seizure-induced synaptotagmin gene identified by differential display. *Proc. Natl. Acad. Sci. U. S. A.* **94**, 2638–2641
47. von Poser, C., Ichtchenko, K., Shao, X., Rizo, J., and Sudhof, T. C. (1997) The evolutionary pressure to inactivate. A subclass of synaptotagmins with an amino acid substitution that abolishes Ca2+ binding. *J. Biol. Chem.* **272**, 14314–14319
48. Li, C., Ullrich, B., Zhang, J. Z., Anderson, R. G., Brose, N., and Sudhof, T. C. (1995) Ca(2+)-dependent and -independent activities of neural and non-neural synaptotagmins. *Nature* **375**, 594–599
49. Perin, M. S., Brose, N., Jahn, R., and Sudhof, T. C. (1991) Domain structure of synaptotagmin (p65). *J. Biol. Chem.* **266**, 623–629
50. Han, W., Rhee, J. S., Maximov, A., Lao, Y., Mashimo, T., Rosenmund, C., and Sudhof, T. C. (2004) N-glycosylation is essential for vesicular targeting of synaptotagmin 1. *Neuron* **41**, 85–99
51. Fernandez-Chacon, R., Konigstorfer, A., Gerber, S. H., Garcia, J., Matos, M. F., Stevens, C. F., Brose, N., Rizo, J., Rosenmund, C., and Sudhof, T. C. (2001) Synaptotagmin I functions as a calcium regulator of release probability. *Nature* **410**, 41–49
52. Bello, O. D., Jouannot, O., Chaudhuri, A., Stroeva, E., Coleman, J., Volynski, K. E., Rothman, J. E., and Krishnakumar, S. S. (2018) Synaptotagmin oligomerization is essential for calcium control of regulated exocytosis. *Proc. Natl. Acad. Sci. U. S. A.* **115**, E7624–E7631
53. Hilfiker, S., Pieribone, V. A., Nordstedt, C., Greengard, P., and Czernik, A. J. (1999) Regulation of synaptotagmin I phosphorylation by multiple protein kinases. *J. Neurochem.* **73**, 921–932
54. Popoli, M. (1993) Synaptotagmin is endogenously phosphorylated by Ca2+/calmodulin protein kinase II in synaptic vesicles. *FEBS Lett.* **317**, 85–88
55. de Jong, A. P., Meijer, M., Saarloos, I., Cornelisse, L. N., Toonen, R. F., Sorensen, J. B., and Verhage, M. (2016) Phosphorylation of synaptotagmin-1 controls a post-priming step in PKC-dependent presynaptic plasticity. *Proc. Natl. Acad. Sci. U. S. A.* **113**, 5095–5100
56. Bradberry, M. M., Courtney, N. A., Dominguez, M. J., Lofquist, S. M., Knox, A. T., Sutton, R. B., and Chapman, E. R. (2020) Molecular basis for synaptotagmin-1-associated neurodevelopmental disorder. *Neuron* **107**, 52–64.e7
57. Liu, S., Lau, L., Wei, J., Zhu, D., Zou, S., Sun, H. S., Fu, Y., Liu, F., and Lu, Y. (2004) Expression of Ca(2+)-permeable AMPA receptor channels primes cell death in transient forebrain ischemia. *Neuron* **43**, 43–55
58. Robbins, J. (2001) KCNQ potassium channels: Physiology, pathophysiology, and pharmacology. *Pharmacol. Ther.* **90**, 1–19
59. Wang, H. S., Pan, Z., Shi, W., Brown, B. S., Wymore, R. S., Cohen, I. S., Dixon, J. E., and McKinnon, D. (1998) KCNQ2 and KCNQ3 potassium channel subunits: Molecular correlates of the M-channel. *Science* **282**, 1890–1893
60. Cooper, E. C., Harrington, E., Jan, Y. N., and Jan, L. Y. (2001) M channel KCNQ2 subunits are localized to key sites for control of neuronal network oscillations and synchronization in mouse brain. *J. Neurosci.* **21**, 9529–9540
61. Shah, M., Mistry, M., Marsh, S. J., Brown, D. A., and Delmas, P. (2002) Molecular correlates of the M-current in cultured rat hippocampal neurons. *J. Physiol.* **544**, 29–37
62. Castaldo, P., del Giudice, E. M., Coppola, G., Pascotto, A., Annunziato, L., and Taglialatela, M. (2002) Benign familial neonatal convulsions caused by altered gating of KCNQ2/KCNQ3 potassium channels. *J. Neurosci.* **22**, RC199
63. Leung, Y. M., Kang, Y., Gao, X., Xia, F., Xie, H., Sheu, L., Tsuk, S., Lotan, I., Tsushima, R. G., and Gaisano, H. Y. (2003) Syntaxin 1A binds to the cytoplasmic C terminus of Kv2.1 to regulate channel gating and trafficking. *J. Biol. Chem.* **278**, 17532–17538
64. Michaelevski, I., Chikvashvili, D., Tsuk, S., Singer-Lahat, D., Kang, Y., Linial, M., Gaisano, H. Y., Fili, O., and Lotan, I. (2003) Direct interaction of target SNAREs with the Kv2.1 channel. Modal regulation of channel activation and inactivation gating. *J. Biol. Chem.* **278**, 34320–34330
65. Tsuk, S., Michaelevski, I., Bentley, G. N., Joho, R. H., Chikvashvili, D., and Lotan, I. (2005) Kv2.1 channel activation and inactivation is influenced by physical interactions of both syntaxin 1A and the syntaxin 1A/soluble N-ethylmaleimide-sensitive factor-25 (t-SNARE) complex with the C terminus of the channel. *Mol. Pharmacol.* **67**, 480–488

66. Miceli, F., Soldovieri, M. V., Ambrosino, P., Barrese, V., Migliore, M., Cilio, M. R., and Taglialatela, M. (2013) Genotype-phenotype correlations in neonatal epilepsies caused by mutations in the voltage sensor of K(v)7.2 potassium channel subunits. *Proc. Natl. Acad. Sci. U. S. A.* **110**, 4386–4391
67. Crumpton, M. J., and Dedman, J. R. (1990) Protein terminology tangle. *Nature* **345**, 212
68. Enrich, C., Rentero, C., de Muga, S. V., Reverter, M., Mulay, V., Wood, P., Koese, M., and Grewal, T. (2011) Annexin A6-linking Ca(2+) signaling with cholesterol transport. *Biochim. Biophys. Acta* **1813**, 935–947
69. Eberhard, D. A., Brown, M. D., and VandenBerg, S. R. (1994) Alterations of annexin expression in pathological neuronal and glial reactions. Immunohistochemical localization of annexins I, II (p36 and p11 subunits), IV, and VI in the human hippocampus. *Am. J. Pathol.* **145**, 640–649
70. Inui, M., Watanabe, T., and Sobue, K. (1994) Annexin VI binds to a synaptic vesicle protein, synapsin I. *J. Neurochem.* **63**, 1917–1923
71. Monastyrskaya, K., Tschumi, F., Babiychuk, E. B., Stroka, D., and Draeger, A. (2008) Annexins sense changes in intracellular pH during hypoxia. *Biochem. J.* **409**, 65–75